A strong broadband 21 cm cosmological signal from dark matter spin-flip interactions

Mansi Dhuria,[a,c] **Viraj Karambelkar,**[b,c] **Vikram Rentala,**[c] **and Priyanka Sarmah**[c]

[a]Basic Sciences Department, Institute of Infrastructure, Technology, Research And Management, Near Khokhra Circle, Maninagar (East), Ahmedabad-380026, Gujarat, India

[b]Cahill Center for Astronomy, California Institute of Technology, 1216 E California Blvd. Pasadena, CA 91106, USA

[c]Department of Physics, Indian Institute of Technology Bombay, Powai, Mumbai, Maharashtra, 400076, India

E-mail: mansidhuria@iitram.ac.in, viraj@astro.caltech.edu, rentala@phy.iitb.ac.in, sarmahpriyanka07@gmail.com

Abstract. In the standard cosmology, it is believed that there are two relatively weak and distinct band-limited absorption features, near 20 MHz ($z \sim 70$) and 90 MHz ($z \sim 15$) in the global cosmological 21 cm signal which are signatures of collisional gas dynamics in the cosmic dark ages and Lyman-α photons from the first stars at cosmic dawn, respectively. A similar prediction of two distinct band-limited, but stronger, absorption features is expected in models with excess gas cooling, which have been invoked to explain the anomalous EDGES signal. In this work, we explore a novel mechanism, where dark matter spin-flip interactions with electrons through a light axial-vector mediator could directly induce a 21 cm absorption signal which is characteristically different from either of these. We find generically, that our model predicts a strong, broadband absorption signal extending from frequencies as low as 1.4 MHz ($z \sim 1000$), from early in the cosmic dark ages where no conventional signal is expected, all the way up to 90 MHz, depending upon the epoch of star formation and X-ray heating. We find a rich set of spectral features that could be probed in current and future experiments looking for the global 21 cm signal. In the standard cosmology and in excess gas cooling models it is expected that the gas spin temperature as inferred from the absorption signal is a tracer of the gas kinetic temperature. However, in our model we find in certain regions of parameter space that the spin temperature and kinetic temperature of the gas evolve differently, and the absorption signal only measures the spin temperature evolution. Large swathes of our model parameter space of interest are safe from existing particle physics constraints, however future searches for short range spin-dependent forces between electrons on the millimeter to nanometer scale have the potential to discover the light mediator responsible for our predicted signal.

Contents

1   Introduction

Cosmic Microwave Background (CMB) radiation serves as a backlight for the neutral hydrogen in the universe along any line of sight. At any redshift z, the Rayleigh-Jeans tail of the CMB spectrum has 21 cm (1420 MHz) photons which can be absorbed by neutral hydrogen in the hyperfine singlet ground state, exciting it to the triplet state. Alternatively, these photons can also trigger stimulated emission via de-excitation of the triplet states to the ground state of hydrogen. One can measure the net absorption or emission from neutral hydrogen at a redshift z by measuring the intensity of background radiation at frequencies $\nu = 1420/(1 + z)$ MHz.

The observed intensity of 21 cm photons from any redshift z can be expressed in terms of the differential brightness temperature $\delta T_b(\nu)$. The expected value of δT_b can be related to the difference between the spin temperature $T_s(z)$ of neutral hydrogen and the CMB temperature $T_{\rm CMB} = 2.73(1 + z)$ K at the corresponding redshift z as [1],

$$\delta T_b = 27\, x_{HI}(z) \left(\frac{1+z}{10}\right)^{1/2} \left(\frac{\Omega_b h^2}{0.022}\right) \left(\frac{0.14}{\Omega_m h^2}\right)^{1/2} \left(\frac{T_s(z) - T_{\rm CMB}(z)}{T_s(z)}\right) \ \ \text{mK.} \qquad (1.1)$$

Here, the spin-temperature T_s is defined in terms of the relative populations of the triplet and singlet states, such that $n_1/n_0 = 3e^{-\frac{\Delta}{T_s}}$, where $\Delta = (hc)/(k_B\, 21\,{\rm cm}) = 69$ mK $= 5.9\,\mu$eV is a temperature/energy scale corresponding to the hyperfine-splitting and n_1 and n_0 are the number densities of the triplet and singlet states respectively. In the formula above Ω_b and Ω_m are the present-day cosmological baryon and matter density fractions, respectively, and $x_{HI}(z)$ is the redshift dependent fraction of neutral hydrogen, which is ~ 1 during the cosmic dark ages from $z \sim 1000$ to $z \sim 10$.

In standard cosmology, the spin temperature is coupled to the CMB temperature and the gas temperature through the relation [2, 3],

$$T_s^{-1} = \frac{T_{\rm CMB}^{-1} + x_C T_K^{-1} + x_\alpha T_c^{-1}}{1 + x_C + x_\alpha}, \qquad (1.2)$$

where T_K is the gas kinetic temperature and T_c (which can be taken to be $\sim T_K$) is the "color temperature" of Lyman-α (Ly-α) photons from the first stars [4]. The effective coupling to T_K due to collisions between the gas molecules is denoted as x_C and the coupling to T_c due to Ly-α photons is denoted as x_α.

At very high redshifts $z \gtrsim 200$, the gas is tightly kinetically coupled to the CMB temperature through the residual free electrons and the collisional coupling x_C is dominant – latching the spin temperature on to the gas temperature, resulting in no net absorption signal. However, near $z \sim 150$ ($\nu \simeq 10$ MHz), the gas decouples from the CMB and begins to cool adiabatically (as $\sim (1 + z)^2$, which is faster than the CMB cooling rate which scales as $(1 + z)$). For a while, the collisional coupling continues to keep the spin temperature coupled to the gas temperature, and this combined with the cold gas temperature results in an absorption dip in the brightness temperature near $z \sim 150$. The collisional coupling becomes less dominant than the coupling to the CMB near $z \sim 50$ ($\nu \simeq 30$ MHz), and the spin temperature rises back up to the CMB temperature once again, leading to a distinct absorption dip extending from approximately 10 to 30 MHz. Meanwhile, the gas continues to cool adiabatically. Near a redshift $z \sim 15$ ($\nu \simeq 90$ MHz), it is expected that Ly-α photons from the first stars once again couple the spin temperature to the gas temperature through

the Wouthuysen-Field effect [2, 5], resulting in a second absorption dip. This absorption dip ends due to X-ray heating of the gas, which raises its temperature above the CMB temperature, which could also potentially give rise to an emission signal, depending upon the history of reionization due to the first sources.

Thus, there is a robust prediction of two distinct absorption dips in the global 21 cm brightness temperature. The first extends from $\nu \sim 10 - 30$ MHz ($z \sim 46 - 140$) due to gas collisional dynamics, and is relatively shallow, since the gas has only just started cooling adiabatically at these redshifts. The second feature near $\nu \sim 90$ MHz ($z \sim 15$) is due to Ly-α photons from the first stars, and is deeper, since the gas has cooled much more. However, the magnitude of the second absorption dip is also tightly constrained by the gas cooling history and is expected to lead to an absorption dip no less than about $\delta T_b \sim -300$ mK at 90 MHz. Both these absorption features are expected to be band-limited, since for the first feature, the collisional coupling turns off shortly after the gas starts cooling adiabatically, and for the second feature, X-ray heating is expected to accompany the turn on of the first stars.

The prediction of two distinct, band-limited, and relatively weak absorption signals is thus a fairly robust prediction of the standard cosmology[1]. Although the exact astrophysics of the first Ly-α photons and X-ray sources remains a matter of speculation, it is expected that detailed observations of the 21 cm signal will allow us to characterize this physics.

A large number of radio telescope experiments such as EDGES [9], PRIZM [10], REACH [11], SARAS [12, 13], SCI-HI [14], BIGHORNS [15] are looking for a global (isotropic, redshift-dependent) 21 cm signal up to a redshift $z \sim 15$, near the epoch of reionization. Other experiments are looking for a signal from higher redshifts going deeper into the cosmic dark ages such as LEDA [16] (up to $z \sim 46$) and the proposed satellite constellation DAPPER [17] (up to $z \sim 80$). Proposals for space-based missions operating on the far side of the moon such as FARSIDE [18], PRATUSH [19], DARE [20], and a possible future iteration of the pathfinder Netherlands-China Low-Frequency Explorer (NCLE) [21] would ultimately have the best sensitivity and potential to probe all the way up to $z \sim 1000$ right up till the era of recombination [22, 23].

In addition to the global signal, several other experiments are looking for 21 cm anisotropies which are expected to unveil the detailed history of reionization such as LOFAR [24], PA-PER [25], MWA [26], 21CMA [27], OVRO-LWA [28], GMRT [29] and HERA [30], with the future to be led by the Square Kilometer Array (SKA) [31, 32].

The EDGES experiment has already claimed a detection of anomalous absorption in the global 21 cm signal with strength $\delta T_b \simeq -500$ mK at 78 MHz ($z \simeq 17$) [33], which is twice as deep as the maximum expected absorption in the standard cosmology. This claim led to intense speculation of exotic physics beyond the Standard Model of particle physics that could explain the anomaly. These explanations were based on the following possibilities: a) the absorption dip is due to anomalous gas cooling due to interactions with dark matter [34–44], b) there is a modification of the Rayleigh-Jeans portion of the CMB spectrum from the standard expectation [45–49] or c) the free electron fraction is smaller than expected and thus the gas decouples from the CMB earlier, leading to a longer epoch of adiabatic cooling [50].

All these models still predict the same *band-limited* (albeit stronger) absorption features in the global signal, due to transition features which are still controlled by the same collisional gas dynamics and Ly-α couplings as in the standard cosmology.

---

[1]For a more detailed discussion of the physics of the spin temperature and predicted 21 cm signal in the standard cosmology, we direct the reader to refs. [3, 6–8].

However, it has been debated whether the observed EDGES signal is really a signature of the first stars or is a spurious detection. In ref. [51], the authors have questioned whether the EDGES observation can be claimed to be an unambiguous detection of a cosmological 21 cm signal by arguing that attempts to fit the purported signal lead to unphysical fit parameters for the foreground emission model.

In light of these experiments (and whether or not the EDGES signal is really cosmological), it is worthwhile to ask if there are alternative predictions of the cosmological global 21 cm signal that could be tested in the near future. A recent attempt at such a prediction has been made in the literature in ref. [52], which has predicted spectral edges and endpoints in 21 cm measurements resulting from resonant dark-photon to visible-photon conversions which would alter the Rayleigh-Jeans tail of the CMB.

In this work, we explore a different possible modification of the global 21 cm signal in a model where dark matter interactions with electrons through an axial-vector mediator could lead to direct spin-flips of the hydrogen atoms through collisions with dark matter particles. This interaction would directly alter the *spin-temperature of the gas*, rather than the distribution of CMB photons. We find generically, that such an interaction would lower the spin-temperature over a large redshift range, leading to a strong, broadband absorption signal from the cosmic dark ages. We will discuss the reasoning for this generic prediction below.

The spin-flip interactions proposed in our work could lead to two effects. The first is a coupling of the spin temperature to a new effective temperature scale T_{eff}, which is in general colder than the gas temperature. We will show that the spin-flip interaction leads to a modification of eq. 1.2 to

$$T_s^{-1} = \frac{T_{\text{CMB}}^{-1} + x_C T_K^{-1} + x_\alpha T_c^{-1} + x_D T_{\text{eff}}^{-1}}{1 + x_C + x_\alpha + x_D}, \tag{1.3}$$

where x_D is the effective coupling of the spin temperature to $T_{\text{eff}} \equiv \mu \left(\frac{T_K}{m_H} + \frac{T_\chi}{m_\chi} \right)$, where μ is the reduced mass of the dark matter (with mass m_χ) and the hydrogen gas (m_H), and T_χ is the dark matter temperature. The second effect of the spin-flip interactions is a cooling of the gas, due to transfer of kinetic energy to the dark matter.

It is the interplay between the cosmological relevance of these two effects that leads to a distinct prediction for the absorption signal. We find a hierarchy between the spin-flip transition rate and the kinetic energy transfer rate which guarantees that the former is always significantly larger. The parameter space of the dark sector model which leads to distinct cosmological signatures can thus be split into three scenarios of a) strong coupling – where both spin-flip interactions and kinetic energy transfer are cosmologically relevant b) weak coupling – where kinetic energy transfer is irrelevant, but spin-flip interactions are important and c) intermediate coupling – which represents a transition region between the other two scenarios.

The dominance of the spin-flip interaction rate is the key feature that distinguishes our model from other models with excess cooling of the gas. Models with only excess gas cooling, lead to deeper absorption dips, which are still band-limited since the transition features are due to the same dynamics (collisional couplings and Ly-α photons) as in the standard cosmology.

In our model, unlike in the excess cooling only models, the dominance of the spin-flip coupling x_D, and a low temperature scale T_{eff}, which is smaller than T_{CMB} through the bulk of the cosmic dark ages, lead to a prediction of a single, strong, broadband absorption trough. The absorption trough is predicted to begin at frequencies as low as 1.4 MHz ($z \sim 1000$) – a region of frequencies from which no absorption signal is expected in the standard cosmology – and extends all the way up to 90 MHz ($z \sim 15$), where our signal merges with that of the standard absorption feature due to the first stars and X-ray sources. The signal is also expected to be very strong compared to standard predictions, since the new temperature scale T_{eff} is much colder at a given redshift than the corresponding T_K in the standard cosmology.

In the specific case of the weak coupling scenario, for sufficiently low DM masses, $T_{\text{eff}} \simeq T_\chi$ and the spin-temperature latches on to the low DM temperature. In the limit of extreme weak coupling, we find that kinetic energy transfer is negligible and the gas cools no more than usual as compared to the standard cosmology. While in the standard cosmology and in excess gas cooling models, any absorption signal is expected to be a tracer of the gas kinetic temperature (as suggested by eq. 1.2), the absorption feature predicted in the weak coupling scenario of our model would only be a tracer of the gas spin temperature (and hence the DM temperature), and it would not measure the gas kinetic temperature.

A few papers have attempted to explain the EDGES absorption signal using dark matter spin-flip interactions. A set of papers on axion Bose-Einstein condensate with spin-flip interactions was considered in [53, 54]. However, [54] claimed that such a condensate would be too weakly coupled to affect the spin-flip. A model similar to ours was studied in the context of the EDGES signal in ref. [55], however in addition to our primary objective – which is to explore the implications for the 21 cm signal, rather than explain the EDGES signal – our calculational methods and parameter space of interest differ significantly from this work.

In our analysis, we focus on regions of parameter space that have strong absorption at $z \sim 17$, consistent with the magnitude of the signal $\delta T_b(z = 17) \simeq -500$ mK claimed by the EDGES collaboration. However, this value is only taken as a benchmark point to which we "pin" our absorption signal, we make no demands on the shape of the absorption signal.

We list some of the key new methods of our paper below:

- We make an accurate Born level bound-state calculation of both the spin-flip scattering cross-section through a light-mediator, which determines the coupling x_D and we also calculate the energy-transfer cross-section, which determines the temperature evolution of the gas.

- Our calculation demonstrates that the thermally averaged bound state cross-section scales as $1/\Delta^2$, where Δ is the tiny hyperfine splitting, allowing for large spin-flip interactions even for relatively weak couplings between electrons and the new mediator.

- We demonstrate the existence of a hierarchy between the spin-flip rate and the energy transfer rate, which leads to the three different predicted scenarios of strong, weak and intermediate couplings discussed previously.

- We find that several regions of the model parameter space which lead to a broadband absorption signal are safe from all laboratory constraints. We argue that various astrophysical and cosmological constraints may be evaded under simple extensions of the

model. We find interesting regions of parameter space which present promising targets for searches for novel short-range spin-dependent interactions for electrons on the millimeter to nanometer scale.

This paper is organized as follows. In sec. 2, we present an effective Lagrangian for our dark matter model interacting with electrons via a light axial-vector mediator. In sec. 3, we show how eq. 1.3 for the spin temperature evolution follows from our model, and present a relationship between the parameter x_D and our Lagrangian parameters. The same spin-flip interaction leads to energy transfer between the dark matter and hydrogen and this in general leads to a coupled temperature evolution of both fluids in the post-recombination era. We discuss the temperature evolution equations in sec. 4. In sec. 5, we present our main results. We classify our parameter space into three distinct regions and discuss the signatures of the global 21 cm signal in each regime. In sec. 6, we clarify some of our assumptions and discuss how changes in these assumptions would change our results. We also discuss the validity of our approximations. In sec. 7, we discuss a variety of constraints on our model and show that there is a large region of our benchmark parameter space that is as yet unconstrained by experimental searches. Finally, we summarize our findings and discuss some future direction in sec. 8. We have shown the details of our calculation of the cross-section for the spin-flip interaction, energy transfer cross-section and some other cross-sections of interest in the appendices.

2 Dark matter model and spin-flip interactions

We present here our model which consists of a dark matter particle χ, which we take to be a Dirac fermion, and a light pseudo-vector mediator particle, which we denote as V, which couples to both the dark matter and electrons with coupling strengths g_χ and g_e, respectively. The relevant interaction terms in our effective Lagrangian are given by,

$$\mathcal{L} = ig_\chi \overline{\chi} \gamma^\mu \gamma^5 \chi V_\mu + ig_e \overline{e} \gamma^\mu \gamma^5 e V_\mu. \tag{2.1}$$

Thus the model has four new parameters, the two coupling constants and the masses of the dark matter and mediator particles, which we denote as m_χ and m_V, respectively.

We assume that the dark matter particle χ is produced asymmetrically in the early universe, with no $\overline{\chi}$ particles surviving as relics. We allow for the possibility that the particle χ that we have considered here makes up only a fraction f of the total DM relic density, which introduces a fifth parameter into our theory.

The interaction between dark matter and neutral hydrogen atoms proceeds through t-channel exchange of the mediator and gives rise to the spin-flip reactions,

$$\chi + H_0 \rightleftarrows \chi + H_1, \tag{2.2}$$

where H_0 denotes neutral hydrogen in the singlet ground state and H_1 denotes the triplet state. The forward reaction is for excitations and the reverse for the de-excitation process. In addition to flipping the spin of the hydrogen atoms, these reactions also transfer energy between the gas and the dark matter particles and could modify the evolution of the gas and DM kinetic temperatures (and hence T_{eff}).

3 Spin-flip interaction rate and the coupling x_D

At any redshift the balance between excitation and de-excitation processes for neutral hydrogen leads to the relationship between the reaction rates [53–55],

$$n_0(B_{01} + C_{01} + P_{01} + D_{01}) = n_1(A_{10} + B_{10} + C_{10} + P_{10} + D_{10}) \tag{3.1}$$

where on the left-hand side B_{01}, C_{01}, P_{01} and D_{01} are redshift dependent rate coefficients (with units of inverse time) for excitation through stimulated interaction with CMB photons, collisional excitations, Ly-α excitations and dark matter scattering induced excitations, respectively. Similarly, the coefficients with subscripts reversed on the right hand side denote the corresponding de-excitation rates. $A_{10} = 2.85 \times 10^{-15}$ s^{-1} $= 1.88 \times 10^{-39}$ GeV is the decay width for the spontaneous electromagnetic decay process of the triplet state into the singlet state. All coefficients other than A_{10} are a result of scattering and can be written as the product of a number density of scattering targets and the thermally averaged cross-section times velocity for the corresponding excitation or de-excitation process. For example, $D_{10} = n_\chi \langle \sigma_{10} v \rangle$, where n_χ is the number density of dark matter particles, and $\langle \sigma_{10} v \rangle$ is the thermal velocity averaged cross-section for the process $\chi + H_1 \to \chi + H_0$.

The principle of detailed balance can be invoked to determine the ratio between the coefficients for excitation and de-excitation for individual processes. For example, we can use the principle of detailed balance in a closed box of temperature T in which only photon induced processes are at play to determine the ratios B_{10}/A_{10} and B_{10}/B_{01}.

We define the modified coefficients $A = \mathcal{A}$, $B = n_\gamma \mathcal{B}$, where $n_\gamma = \frac{\Delta^3}{2\pi^2} \frac{1}{e^{\frac{\Delta}{T}}-1} \equiv F(\Delta)\frac{1}{e^{\frac{\Delta}{T}}-1}$ is the number density of 21 cm photons and $\Delta = 5.9$ μeV is the 21 cm energy scale. We then obtain the relation,

$$n_0 n_\gamma \mathcal{B}_{01} = n_1(\mathcal{A}_{10} + n_\gamma \mathcal{B}_{10}), \tag{3.2}$$

which implies

$$\mathcal{B}_{01} = 3e^{-\Delta/T}\left(\frac{\mathcal{A}_{10}}{n_\gamma} + \mathcal{B}_{10}\right). \tag{3.3}$$

This relationship for forward and backward rates must hold true for any temperature T. Since $\mathcal{A}_{10}$, $\mathcal{B}_{10}$, and $\mathcal{B}_{01}$ are temperature independent quantities[2], this in turn implies that,

$$\frac{\mathcal{B}_{01}}{\mathcal{B}_{10}} = 3 \tag{3.4}$$

and

$$\frac{\mathcal{A}_{10}}{\mathcal{B}_{10}} = F(\Delta) = \frac{\Delta^3}{2\pi^2}. \tag{3.5}$$

These are well known relations for the standard Einstein coefficients $\mathcal{A}_{10}$ and $\mathcal{B}_{10}$.

---

[2]$\mathcal{A}_{10}$ is the natural decay width and is obviously temperature independent. $\mathcal{B}_{01}$ ($\mathcal{B}_{10}$) is equal to the velocity averaged photon excitation (de-excitation) cross-section multiplied by the velocity $\langle \sigma v \rangle$, which is temperature independent for s-wave processes.

Returning to the rates for the original cosmological system, we find upon plugging in the expressions for the Einstein coefficients that the de-excitation rate is given by

$$B_{10} = n_\gamma \mathcal{B}_{10} \simeq A_{10} \frac{T_{\text{CMB}}}{\Delta}, \tag{3.6}$$

$$= 8.28 \times 10^{-37} \left(\frac{1+z}{1+10} \right) \text{ GeV}, \tag{3.7}$$

$$= 1.26 \times 10^{-12} \left(\frac{1+z}{1+10} \right) \text{ s}^{-1}, \tag{3.8}$$

and the excitation rate $B_{01} = 3B_{10}$.

One can apply similar reasoning to the collisional processes (due to collisions of neutral hydrogen with either other H atoms, electrons or protons) and also to the Ly-α processes to obtain the relations,

$$\frac{C_{01}}{C_{10}} = 3e^{-\Delta/T_K} \simeq 3 \left(1 - \frac{\Delta}{T_K} \right), \tag{3.9}$$

$$\frac{P_{01}}{P_{10}} = 3e^{-\Delta/T_c} \simeq 3 \left(1 - \frac{\Delta}{T_c} \right), \tag{3.10}$$

where T_K is the kinetic temperature of the gas, and T_c is the color temperature of Ly-α radiation, both of which are typically much larger than the hyperfine splitting Δ.

We cannot simply use the principle of detailed balance to get the ratio of rate coefficients for dark matter excitations D_{01} and de-excitations D_{10}, because the kinetic temperature of the DM and gas are different in general. We explicitly work out these rates in the appendix and we show that the ratio is given by,

$$\frac{D_{01}}{D_{10}} = 3e^{-\Delta/T_{\text{eff}}} \simeq 3 \left(1 - \frac{\Delta}{T_{\text{eff}}} \right), \tag{3.11}$$

where $T_{\text{eff}} = \mu \left(\frac{T_K}{m_H} + \frac{T_\chi}{m_\chi} \right)$, and $\mu = \frac{m_H m_\chi}{m_H + m_\chi}$ is the reduced mass of the dark matter and the hydrogen gas. Intuitively, the threshold energy needed for excitation reactions leads to the exponential Boltzmann suppression factor of the excitation rate relative to the de-excitation rate.

Using all of the above ratios of rate coefficients, we find an expression for the spin-temperature,

$$T_s^{-1} = \frac{T_{\text{CMB}}^{-1} + x_C T_K^{-1} + x_\alpha T_c^{-1} + x_D T_{\text{eff}}^{-1}}{1 + x_C + x_\alpha + x_D}, \tag{3.12}$$

where $x_\alpha = \frac{C_{10}}{B_{10}}$ and $x_C = \frac{P_{10}}{B_{10}}$ and $x_D = \frac{D_{10}}{B_{10}}$ are effective couplings of the spin-temperature to the gas, Ly-α photons and dark matter respectively. The coupling x_D to the temperature scale T_{eff} is a direct consequence of the spin-dependent interaction between electrons and dark matter. Thus, we see that there is another temperature scale that the spin temperature can couple to when DM spin-flip interactions dominate the hyperfine transitions.

If we know how the gas and DM temperatures evolve with time (or redshift) and if we also know how the effective couplings x_C, x_α and x_D change with redshift, then we can determine the spin temperature at any epoch.

We have evaluated the cross-section for the excitation and de-excitation processes $\chi + H_0 \rightleftarrows \chi + H_1$ in appendix A.2. This scattering process has a large cross-section which

arises because of the usual forward scattering divergence of a light mediator exchanged in the t-channel. For sufficiently light mediator masses, the divergence is cut-off, not by the mediator mass, but rather by the tiny inelastic mass-splitting Δ between the singlet and triplet states. Our detailed calculation of the cross-section in the regime of light mediator mass shows that the thermally averaged bound state cross-section is of the form $\sigma_{01} \sim \frac{3}{4\pi} \frac{g_\chi^2 g_e^2}{\Delta^2}$, which leads to a large interaction rate even for relatively weak couplings.

In the appendix, we show that the de-excitation rate

$$D_{10} = 3.01 \times 10^{-12} \left(\frac{f}{0.1}\right) \left(\frac{0.1 \text{ GeV}}{m_\chi}\right) \left(\frac{\alpha_\chi}{10^{-2}}\right) \left(\frac{\alpha_e}{10^{-14}}\right) \left(\frac{0.1 \text{ GeV}}{\mu}\right)^{\frac{1}{2}} \left(\frac{T_{\text{eff}}}{10 \text{ K}}\right)^{\frac{1}{2}} \left(\frac{1+z}{1+10}\right)^3 \text{ s}^{-1},$$

$$(3.13)$$

where $\alpha_\chi = \frac{g_\chi^2}{4\pi}$ and $\alpha_e = \frac{g_e^2}{4\pi}$.

Taking the ratio of the expression for D_{10} above, with the rate B_{10} in eq. 3.8, we find an expression for the coupling of the spin temperature to the effective temperature as,

$$x_D = 2.4 \left(\frac{f}{0.1}\right) \left(\frac{0.1 \text{ GeV}}{m_\chi}\right) \left(\frac{\alpha_\chi}{10^{-2}}\right) \left(\frac{\alpha_e}{10^{-14}}\right) \left(\frac{0.1 \text{ GeV}}{\mu}\right)^{\frac{1}{2}} \left(\frac{T_{\text{eff}}}{10 \text{ K}}\right)^{\frac{1}{2}} \left(\frac{1+z}{1+10}\right)^2. \quad (3.14)$$

4   Temperature evolution equations

The evolution of the dark matter and neutral hydrogen gas temperatures are given by the following coupled Boltzmann equations (appendix A.3):

$$\frac{dT_\chi}{d\log(1+z)} = +2T_\chi - \frac{2}{3}\frac{\Gamma_\chi}{H}(T_K - T_\chi), \quad (4.1)$$

$$\frac{dT_K}{d\log(1+z)} = +2T_K - \frac{\Gamma_c}{H}(T_{\text{CMB}} - T_K) - \frac{2}{3}\frac{\Gamma_H}{H}(T_\chi - T_K). \quad (4.2)$$

These equations are valid in the epoch prior to the cosmic dawn, before X-ray heating from the first sources turns on. The first terms on the right hand side of these equations correspond to adiabatic non-relativistic cooling of the dark matter and the gas, respectively, due to the expansion of the universe. The rate Γ_c is the compton rate which couples the gas to the CMB temperature through the residual free electron fraction $x_e(z)$ and is given by [56, 57],

$$\Gamma_c = \frac{8a_r\sigma_T}{3m_e c}T_{\text{CMB}}^4(z)\frac{x_e(z)}{(1+0.08+x_e(z))} \quad (4.3)$$

$$= 7.4 \times 10^{-20} \left(\frac{1+z}{1+10}\right)^4 \times \frac{x_e(z)}{2 \times 10^{-4}}\frac{1.08}{(1+0.08+x_e(z))} s^{-1}. \quad (4.4)$$

In this expression $m_e = 0.511 \text{ MeV}/c^2$ is the electron mass, $a_r = 4.72 \times 10^{-3} \text{ MeV m}^{-3} \text{ K}^{-4}$ is the radiation constant and $\sigma_T = 6.65 \times 10^{-29} \text{ m}^2$ is the Thomson scattering cross-section for free-electrons with the CMB. The compton rate depends on the free electron fraction $x_e(z)$ which must be solved for in a given cosmology. Since we have assumed that our DM is asymmetric, it does not self-annihilate. Therefore, the physics of recombination or the ionization fraction history $x_e(z)$ are both unaltered from the standard cosmology. In our numerical simulations in sec. 5 we use the code HyRec [56] to compute the free electron fraction.

The rates Γ_χ and Γ_H are the heating rates for DM and the gas respectively, which can be thought of as the inverse time-scale for transfer of an $\mathcal{O}(1)$ fraction of their kinetic energy to one another. Schematically these rates are of the form $\Gamma \sim n\langle\bar{\sigma}v\rangle$, where n is the number density of targets and $\langle\bar{\sigma}v\rangle$ is thermally averaged "energy-transfer cross-section".

In appendix A.3 we evaluate the energy transfer cross-sections and derive the temperature evolution eqs. 4.1 and 4.2. We argue that the energy transfer cross-section is dominated by the inelastic scattering process $\chi + H_0 \leftrightarrows \chi + H_1$ rather than by elastic scattering processes. This is because the forward divergence of the inelastic scattering, which is cut-off by the hyperfine mass-splitting, diverges as $\frac{1}{\Delta}$, whereas the divergence of elastic scattering, which is cut-off by the mediator mass, is only enhanced as $\text{Log } m_V$.

The detailed expressions for the rates Γ_χ and Γ_H are of the form (appendix A.3),

$$\Gamma_H = 3.11 \times 10^{-15} \left(\frac{f}{0.1}\right) \left(\frac{0.1 \text{ GeV}}{m_\chi}\right) \left(\frac{\alpha_\chi}{10^{-2}}\right) \left(\frac{\alpha_e}{10^{-14}}\right) \left(\frac{1 \text{ GeV}}{M}\right) \left(\frac{\mu}{0.1 \text{ GeV}}\right)^{\frac{1}{2}} \left(\frac{10 \text{ K}}{T_{\text{eff}}}\right)^{\frac{1}{2}} \left(\frac{1+z}{1+10}\right)^3 \text{ s}^{-1},$$
$$(4.5)$$

$$\Gamma_\chi = 6.02 \times 10^{-16} \left(\frac{\alpha_\chi}{10^{-2}}\right) \left(\frac{\alpha_e}{10^{-14}}\right) \left(\frac{1 \text{ GeV}}{M}\right) \left(\frac{\mu}{0.1 \text{ GeV}}\right)^{\frac{1}{2}} \left(\frac{10 \text{ K}}{T_{\text{eff}}}\right)^{\frac{1}{2}} \left(\frac{1+z}{1+10}\right)^3 \text{ s}^{-1},$$
$$(4.6)$$

where $M = m_\chi + m_H$. Since the inelastic scattering process is dominated by forward scattering in which the energy transfer per collision is small, this leads to a suppression of the energy-transfer rate Γ_H relative to the standard excitation/de-excitation rate D_{01} ($\simeq 3D_{10}$) by a factor of $S \equiv \left(\frac{\Delta\mu}{2MT_{\text{eff}}}\right) = 3.42 \times 10^{-4} \left(\frac{10 \text{ K}}{T_{\text{eff}}}\right) \left(\frac{\mu}{0.1 \text{ GeV}}\right) \left(\frac{1 \text{ GeV}}{M}\right)$. Also, the energy transfer rate to the gas Γ_H, is enhanced relative to the energy transfer rate to the DM Γ_χ, by a factor of R, where

$$R \equiv \frac{n_\chi}{n_H} = \frac{f\Omega_{\text{DM}}/m_\chi}{\Omega_b/m_H} = 5.16 \left(\frac{f}{0.1}\right) \left(\frac{0.1 \text{ GeV}}{m_\chi}\right). \qquad (4.7)$$

Here, we have used the present-day total DM density fraction $\Omega_{\text{DM}} = 0.26$ and the baryon density fraction $\Omega_b = 0.05$. For simplicity, we have also assumed that all the baryons are in the form of hydrogen.

The Hubble rate H in our temperature evolution equations is as usual given by,

$$H(z) = H_0\sqrt{\Omega_\Lambda + \Omega_m(1+z)^3 + \Omega_r(1+z)^4}, \qquad (4.8)$$

where $H_0 = 67$ km/s/Mpc is the Hubble constant and $\Omega_m = 0.31$, $\Omega_\Lambda = 0.69$ are the present-day total matter and dark energy density fractions, respectively. All values of the cosmological parameters are taken from Planck data [58]. We take $\Omega_r = 9.6 \times 10^{-5}$ to be the present day radiation density fraction. This value includes the contributions of photons and neutrinos, but does not include possible contributions from the light pseudo-vector mediator to the radiation density in the early universe. The exact value of Ω_r is not so important in the temperature evolution, since for the redshifts of interest $10 \lesssim z \lesssim 1000$ the universe is matter dominated to a good approximation. However, there are observational constraints on extra radiation species, usually parameterized in terms of extra number of effective neutrinos (or ΔN_{eff}). We will discuss this constraint and the implications in more detail in sec. 7.

In the matter dominated era, the Hubble rate has the approximate form,

$$H = H_0 \Omega_m^{1/2} (1 + z)^{3/2}, \tag{4.9}$$

$$= 2.90 \times 10^{-41} \left(\frac{1+z}{1+10} \right)^{\frac{3}{2}} \ \text{GeV}, \tag{4.10}$$

$$= 4.41 \times 10^{-17} \left(\frac{1+z}{1+10} \right)^{\frac{3}{2}} \ \text{s}^{-1}. \tag{4.11}$$

Note on the anomalous EDGES absorption signal in the standard cosmology without dark sector interactions

The rates Γ_c and H are plotted in fig. 4a as a function of z. Since these two rates are the same as in the standard cosmology, one can use them to understand the problem of the anomalous EDGES absorption signal. In the figure, we see that Γ_c drops below H at a decoupling redshift of $z_d \sim 130$. In the standard cosmology, the gas would kinetically decouple from the CMB at a redshift z_d and begin to adiabatically cool. This would lead to a gas temperature of,

$$T_K(z = 17) = T_{\text{CMB}}(z_d) \left(\frac{1+17}{1+z_d} \right)^2, \tag{4.12}$$

$$= 6.8 \left(\frac{1+130}{1+z_d} \right) \text{K}. \tag{4.13}$$

If one assumes a strong Ly-α induced coupling at $z = 17$ to the color temperature (which can be taken to be the same as the gas temperature T_K), then this leads to the lowest possible prediction of the spin temperature $T_s(z = 17) = 6.8$ K, or equivalently a differential brightness temperature $\delta T_b \simeq -227$ mK, which is not enough of an absorption dip to explain the EDGES signal.

In order to obtain $\delta T_b(z = 17) \simeq -500$ mK, we would need a much colder spin temperature of $T_s(z = 17) = 3.32$ K. Such a low spin temperature can not be obtained in the standard cosmology, but can be obtained in models with excess gas cooling, and also in our model, as we shall see in the next section.

5 Method and results

5.1 Predicting the differential brightness temperature evolution with spin-flip interactions

Our goal is to predict the global differential brightness temperature evolution $\delta T_b(z)$ for different parameters of our model. We will then contrast the predictions of our model with those of the standard cosmology, as well as models with excess gas cooling that attempt to explain the EDGES absorption dip.

The inputs to our prediction rely on the following parameters: the coupling product $\alpha_e \alpha_\chi$, the DM mass m_χ and the fraction of DM f that couples to the pseudo-vector mediator. We do not specify the value of the mediator mass, but we assume that it is light enough that the forward scattering divergence of the cross-section for inelastic scattering between the hyperfine states has a cut-off which is dominated by the inelastic mass-splitting parameter Δ rather than by the mediator mass. Under this assumption, our calculations are independent of the mediator mass.

For a given point in the parameter space of our model, our procedure to predict the global 21 cm brightness temperature is as follows:

1. First, we solve the coupled temperature evolution equations 4.1 and 4.2 for $T_K(z)$ and $T_\chi(z)$ given an assumption of the initial conditions on these temperatures. Note that the rate coefficients Γ_χ and Γ_H are functions of the temperature $T_{\text{eff}} = \mu \left(\frac{T_K}{m_H} + \frac{T_\chi}{m_\chi} \right)$, which is a combination of T_χ and T_K. Thus, the equations for temperature evolution are non-linear coupled differential equations and must be solved numerically. However, in some regimes of parameter space, we can predict the asymptotic behavior of the solutions at high and low redshifts and obtain approximate analytic solutions.

2. The solutions to the temperature evolution equations will depend on our assumed initial conditions, which we take at $z = 1000$, near recombination. Our fiducial choice of initial conditions will be to assume $T_K = T_\chi = T_{\text{CMB}} = 2.73 \times (1 + 1000)$ K at $z = 1000$. We will see that for strong couplings, the choice of initial conditions is not important and we get the same predictions regardless of the initial conditions. However for weak couplings, the choice of initial conditions affects our predictions. We will discuss the effect of different choices for the initial conditions and the assumptions they correspond to about pre-recombination physics in sec. 6.

3. Once we know the temperature evolution history of T_K and T_χ, we can predict T_{eff} at all redshifts.

4. In order to predict the spin-temperature evolution using eq. 3.12, we need the evolution of the couplings x_C - the collisional coupling of the spin temperature to the gas kinetic temperature (which is well known, see for e.g. eq 10 in ref [1]), x_α - the Ly-α coupling which depends on the astrophysical assumptions of the formation of first stars and galaxies (see for e.g. [59] and references therein), and also of relevance for the Ly-α coupling we need to know the color temperature (which also depends on the astrophysical model), and x_D - the coupling to the effective temperature T_{eff} (which we have derived, see eq. 3.14).

5. We will assume for simplicity that the astrophysical processes from cosmic dawn, namely Ly-α photons and X-ray heating of the gas, are only relevant at redshifts $z \lesssim 15$, and we will set $x_\alpha = 0$ at higher redshifts. Our predictions of the absorption signal will be limited to the redshift range $15 \lesssim z \lesssim 1000$, or 21 cm frequencies between 1.4 and 89 MHz, to avoid complications of modelling the uncertain astrophysics of the cosmic dawn.

6. After solving the temperature evolution equations, and with knowledge of the coupling coefficients of the spin temperature, we can solve for the spin temperature and brightness temperature over the redshift range of interest.

Since strong absorption signals are a generic feature of our model, as a benchmark, we focus our analysis on the region of parameter space of f, $\alpha_e \alpha_\chi$ and m_χ which lead to a differential brightness temperature $\delta T_b(z = 17) \simeq -500$ mK $(T_s(z = 17) = 3.32$ K), consistent with the magnitude of the signal claimed by the EDGES collaboration at this redshift. In our numerical scan, we allow for some flexibility in this constraint, by relaxing the requirement to -400 mK $\lesssim \delta T_b(z = 17) \lesssim$ -600 mK $(2.7$ K $\lesssim T_s(z = 17) \lesssim 3.9$ K). We

reiterate that our goal is not to explain the EDGES signal, but rather, this point is a useful place to "pin" our predicted absorption spectrum, without making additional demands on the shape of the absorption signal.

The result of a numerical scan, using the procedure outlined above, yields the parameter space of interest, which is shown in fig. 1. In each panel of the figure we show, for different values of $f = 1, 0.1, 0.01, 0.001$ (the dark matter density fraction made up by our dark matter candidate), the allowed values of the coupling product $\alpha_e \alpha_\chi$ and the dark matter mass m_χ that lead to a predicted value of $\delta T_b(z = 17)$ between -400 mK and -600 mK. For each value of f, we find three distinct categories of solutions which are shown in different colors in the figure – 1) strong coupling (green), 2) weak coupling (magenta), and 3) intermediate coupling (blue).

For the strong and weak coupling scenarios, we are also able to obtain approximate analytic solutions to the temperature evolution equations and therefore we can analytically determine the expected parameter space regions which give rise to the benchmark $\delta T_b(z = 17) = -500$ mK. The analytically determined parameter space points are plotted with black lines in fig. 1, and are in good agreement with our numerical results.

In the rest of this section, we will discuss each of the scenarios in turn. As we discuss each scenario, we will first discuss our analytic understanding of the solutions, and then show the comparison with our numerical results. For concreteness, we will take three benchmark points with $f = 0.1$ (shown in the top-right panel of fig. 1) for strong/weak/intermediate couplings when discussing our numerical results.
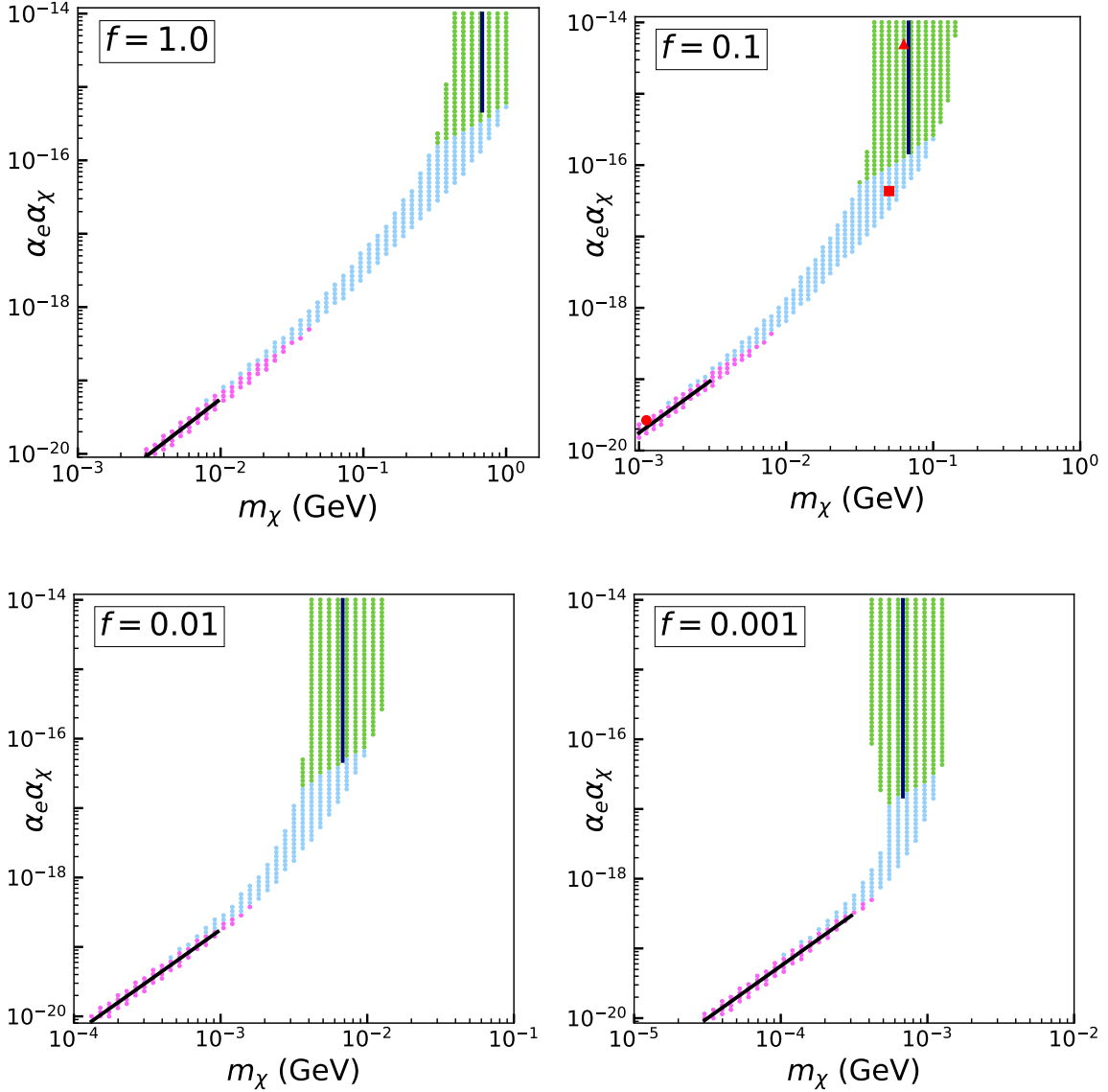
Figure 1: Allowed parameter space of the coupling product $\alpha_e\alpha_\chi$ and the dark matter mass m_χ that leads to a predicted value of $\delta T_b(z = 17)$ between -400 mK and -600 mK. Each panel shows the allowed parameter space for different values of the dark matter density fraction $f = 1, 0.1, 0.01, 0.001$ made up of the dark matter candidate in our model. The allowed parameter space was found by a numerical scan whose procedure is described in the text. The colors green, blue, and magenta of the different regions correspond to strong coupling, intermediate coupling, and weak coupling scenarios, respectively. For comparison, we also show an analytic prediction of the allowed parameter space that leads to $\delta T_b(z = 17) = -500$ mK at strong and weak couplings with black lines. The analytic prediction is in good agreement with the results of our numerical scan. Also for $f = 0.1$ we have shown three benchmark points (in red), one for each scenario, which will be used when presenting detailed numerical results.

5.2 Scenario 1: Strong Coupling

5.2.1 Analytic understanding of strong coupling solutions

When the coupling product $\alpha_\chi \alpha_e$ is sufficiently large, both the spin-flip coupling and kinetic energy transfer rate are large. In such a limit we expect the gas and the DM to behave like a single tightly coupled fluid with a common temperature $T_{\rm eff} = T_\chi = T_K$. We can then multiply the temperature evolution equations for the dark matter and the gas in eq. 4.1 and eq. 4.2 by n_χ and n_H, respectively, and add them together and then take the limit of a common temperature. In this limit we find the following equation for the evolution of $T_{\rm eff}$:

$$\frac{dT_{\rm eff}}{dz} = +\frac{2T_{\rm eff}}{1+z} - \frac{n_H}{n_H + n_\chi}\frac{\Gamma_c}{H(1+z)}(T_{\rm CMB} - T_{\rm eff}), \tag{5.1}$$

$$= +\frac{2T_{\rm eff}}{1+z} - \frac{1}{1+R}\frac{\Gamma_c}{H(1+z)}(T_{\rm CMB} - T_{\rm eff}), \tag{5.2}$$

where $R = \frac{n_\chi}{n_H} = \frac{f\Omega_{\rm DM}}{\Omega_b}\frac{m_H}{m_\chi} = 5.16\frac{f}{0.1}\frac{0.1\,{\rm GeV}}{m_\chi}$. Thus, the combined fluid has an effective coupling rate to the CMB which is given by $\Gamma_c' \equiv \frac{1}{1+R}\Gamma_c$, which is reduced by a factor $\frac{1}{1+R}$ relative to the coupling rate Γ_c of baryons alone. This is because the kinetic energy transferred from the photons to the baryons is redistributed over both the DM and baryons.

In addition, at strong coupling, we have a large spin-flip rate D_{10} which dominates the CMB spin-flip rate B_{10} (i.e. $x_D \gg 1$). The dominance of the DM spin-flip rate over the CMB spin-flip rate ensures that the spin temperature $T_s = T_{\rm eff}$ at $z = 17$. In order to obtain an absorption dip with $\delta T_b(z = 17) \simeq -500$ mK, we would need $T_s(z = 17) = T_{\rm eff}(z = 17) \simeq 3.32$ K in this scenario (using eq. 1.1).

Now the combined DM-gas fluid is tightly coupled to the CMB at early times when $\Gamma_c' > H$ and decouples from the CMB when Γ_c' drops below H at a redshift denoted as z_d. Thereafter, the combined fluid continues to cool adiabatically. Thus, the temperature evolution of $T_{\rm eff}$ in this scenario is as follows,

$$T_{\rm eff}(z) = T_{\rm CMB}(z = 1000)\left(\frac{1+z}{1+1000}\right) \quad \text{for } z > z_d \tag{5.3}$$

$$= T_{\rm CMB}(z = 1000)\left(\frac{1+z_d}{1+1000}\right)\left(\frac{1+z}{1+z_d}\right)^2 \quad \text{for } z < z_d. \tag{5.4}$$

In order to obtain $T_s = T_{\rm eff} = 3.32$ K at $z = 17$, we need $z_d = 265$. We can solve for the DM model parameters needed to obtain this redshift of decoupling by equating $\Gamma_c' = H$ at $z = 265$. Since the rate evolution of Γ_c and H are well known and do not depend on the dark matter physics, this condition determines the value of R, which depends only on m_χ and f, as $R = 7.6$. Using the expression for R, we have the following criteria on the parameter space for solutions with strong coupling:

1. Criteria needed for decoupling of the combined gas-DM system from the CMB at $z_d = 265$

$$m_\chi = 0.68f \text{ GeV} \tag{5.5}$$

Thus, for a given value of the dark matter fraction f, which has spin-flip interactions, the mass of the dark matter for this class of solutions is *uniquely determined*.

In order to ensure that the spin temperature of the gas is coupled to $T_{\rm eff}$, we also need the coupling x_D to be large, i.e. $x_D \gtrsim 10$ at $z = 17$. This criteria can be expressed as:

2. Criteria for large spin-flip coupling rate at $z = 17$

$$\alpha_\chi \alpha_e > 8.6 \times 10^{-16} \frac{1}{f} \frac{m_\chi}{\text{GeV}} \left(\frac{\mu}{\text{GeV}} \right)^{1/2} , \qquad (5.6)$$

For small values of f, the first criteria implies $m_\chi \ll 1$ GeV. Using this limit, we can set $\mu \to m_\chi$ and substitute the value of m_χ from criteria 1 in the second criteria, this gives us:

2′. Modified Criteria for large spin-flip coupling rate at $z = 17$ (valid for small f)

$$\alpha_\chi \alpha_e > 4.8 \times 10^{-16} \sqrt{f}. \qquad (5.7)$$

These two criteria 1 and 2 (or 2′) give us an analytic range of parameters m_χ and $\alpha_\chi \alpha_e$ for a given value of f. We plot this analytic solution in each of the panels of fig. 1. Note that in addition to the criteria on large spin-flip rates, we also need a self-consistency criteria for this solution to ensure tight coupling between the gas and the dark matter fluid. The criteria for self-consistency are given by $\Gamma_H, \Gamma_\chi > H$ at $z = 265$, i.e. the gas and the DM remain tightly coupled to each other till the combined fluid kinetically decouples from the CMB[3]. Since, $\Gamma_H = R\Gamma_\chi$, and since $R > 1$, it is sufficient to look at the self-consistency criteria $\Gamma_\chi > H$ at $z = 265$. Thus, the condition on couplings that we obtain from self-consistency is:

3. Self-consistency criteria for tight kinetic coupling till $z = 265$

$$\alpha_\chi \alpha_e > 1.8 \times 10^{-19} \left(\frac{M}{\text{GeV}} \right) \left(\frac{\text{GeV}}{\mu} \right)^{1/2} , \qquad (5.8)$$

where $M = m_\chi + m_H$. Once again, for small f and substituting criteria 1 for the mass m_χ in terms of f, we obtain:

3′. Modified self-consistency criteria for tight kinetic coupling till $z = 265$ (valid for small f)

$$\alpha_\chi \alpha_e > 2.13 \times 10^{-19} \frac{1}{\sqrt{f}} \qquad (5.9)$$

This criteria is a weaker constraint than criteria 2 (or 2′) for $f > 0.001$, so self-consistency is automatically satisfied in such cases by requiring tight spin-flip coupling.

5.2.2 Numerical results for strong coupling benchmark point

In our numerical scan, in addition to the basic criteria that we had imposed to identify regions of parameter space of interest in the beginning of this section, we impose the requirement that $x_D(z = 17) > 10$ to identify solutions in the strong coupling scenario. We will discuss a particular benchmark point $f = 0.1$, $m_\chi = 0.06$ GeV and $\alpha_e \alpha_\chi = 5 \times 10^{-15}$. In fig. 2a, we show the energy transfer rates Γ_H, Γ_χ and the Hubble rate H as functions of z for this benchmark point. We can see from the figure that the rates Γ_H and Γ_χ are both larger than the Hubble rate throughout the redshift range $10 \lesssim z \lesssim 1000$, indicating that the DM and gas are tightly kinetically coupled to each other. This behaviour is clearly seen in fig. 2b, in which we show the temperature evolution of T_K and T_χ, where both temperatures track each other very closely. In fig. 2a, we also plot the effective "compton coupling rate" of the DM-gas fluid to the CMB (Γ_c'), and we see that this rate decouples (drops below the Hubble rate) at $z = 271$ (near $z = 265$ as predicted by our analytic estimate). In fig. 2b, we

---

[3]Thereafter, for small enough f or m_χ, T_{eff} is dominated by T_χ, so it is sufficient that the DM fluid decouples from the gas any time after $z = 265$.

can see the common temperature evolution of the DM-gas switches from tracking the CMB temperature (and scaling as $(1 + z)$) from $z = 1000$ till $z = 271$, to adiabatic cooling (scaling as $(1 + z)^2$) from $z = 271$ onwards to lower redshifts.

In fig. 2c, we show the evolution of the spin-temperature coupling x_D to the temperature T_{eff} (which is just the same as the common temperature of the DM-gas fluid for strong coupling), and the collisional coupling x_C to the gas temperature T_K. At all redshifts, we see that the coupling $x_D \gg x_C, 1$. This indicates that the DM spin-flip coupling reaction rate D_{10} is the most dominant spin-flip rate over both the collisional coupling rate, as well as the CMB induced spin-flip rate B_{10}. Thus, at all redshifts, and in particular, at $z = 17$, T_s tracks the common temperature of the gas-DM fluid (also shown in fig. 2b). The early decoupling of the gas-DM fluid at $z = 271$ leads to a value of $T_s = T_{\text{eff}} = 3.32$ K at $z = 17$, which yields a differential brightness temperature dip $\delta T_b(z = 17) \simeq -516$ mK.

In fig. 2d, we show the differential brightness temperature as a function of redshift z, inferred from the spin temperature evolution history. Since, $\delta T_b \propto T_s - T_{\text{CMB}}$ and T_s drops faster than T_{CMB} at low redshift, we see that δT_b becomes more negative at lower redshifts, indicating greater absorption at these redshifts. We expect that below some redshift, $z \lesssim 15$, Ly-α coupling to T_K would turn on due to star formation and be the dominant determining coupling of the spin-temperature to the color temperature (or T_K). Moreover X-ray heating would raise T_K, thus leading to a rise in the spin temperature, and also the brightness temperature below some redshift. However, since the details of this would depend on the astrophysical model, we do not show this rise in our figure, but rather our figure is to be taken seriously only above redshifts $z \gtrsim 15$.

In fig. 3 we show, for our strong coupling benchmark point, the predicted differential brightness temperature evolution as a function of redshifted 21 cm frequency. We also show for comparison, in the same figure, the expected signal in the standard cosmology and also in a model with excess gas cooling without spin-flip interactions, with parameters of the latter model chosen to explain the EDGES anomalous absorption dip [60]. We see that in both the standard cosmology and in the excess cooling model, there are two distinct, band-limited absorption features, one at high redshifts (~ 20 MHz), which corresponds to the dominance of collisional coupling of the spin temperature to the gas temperature, and the second at lower redshifts (~ 80-90 MHz), which corresponds to dominance of Ly-α couplings. The model with excess gas cooling, has deeper absorption dips than that of the standard cosmology, but the absorption features are still distinct.

In contradistinction to these signals, our strong coupling benchmark predicts a single, strong, broadband absorption feature that extends from 5.3 MHz ($z = 271$) all the way up to 89 MHz ($z = 15$). At all frequencies in this range, the dip in brightness temperature is caused by spin-flip interactions between the dark matter and neutral hydrogen.

Moreover, in general in the strong coupling scenario, since the spin temperature is controlled by the adiabatically cooling DM-gas fluid temperature, the shape of the absorption signal is very precisely predicted in this frequency range, independently of the exact dark matter mass and couplings and also independently of our assumptions on the initial conditions. In particular, given the strength of the absorption dip at any frequency, for e.g. given $\delta T_b(78 \text{ MHz}, z = 17) = -516$ mK, we can precisely predict the location of the start of the absorption feature at $\nu = 5.3$ MHz ($z = 271$).

At larger frequencies than 89 MHz the signal is expected to rise back up due to a combination of Ly-α photons and X-ray heating. We have not shown this astrophysical model dependent rise in our figure.
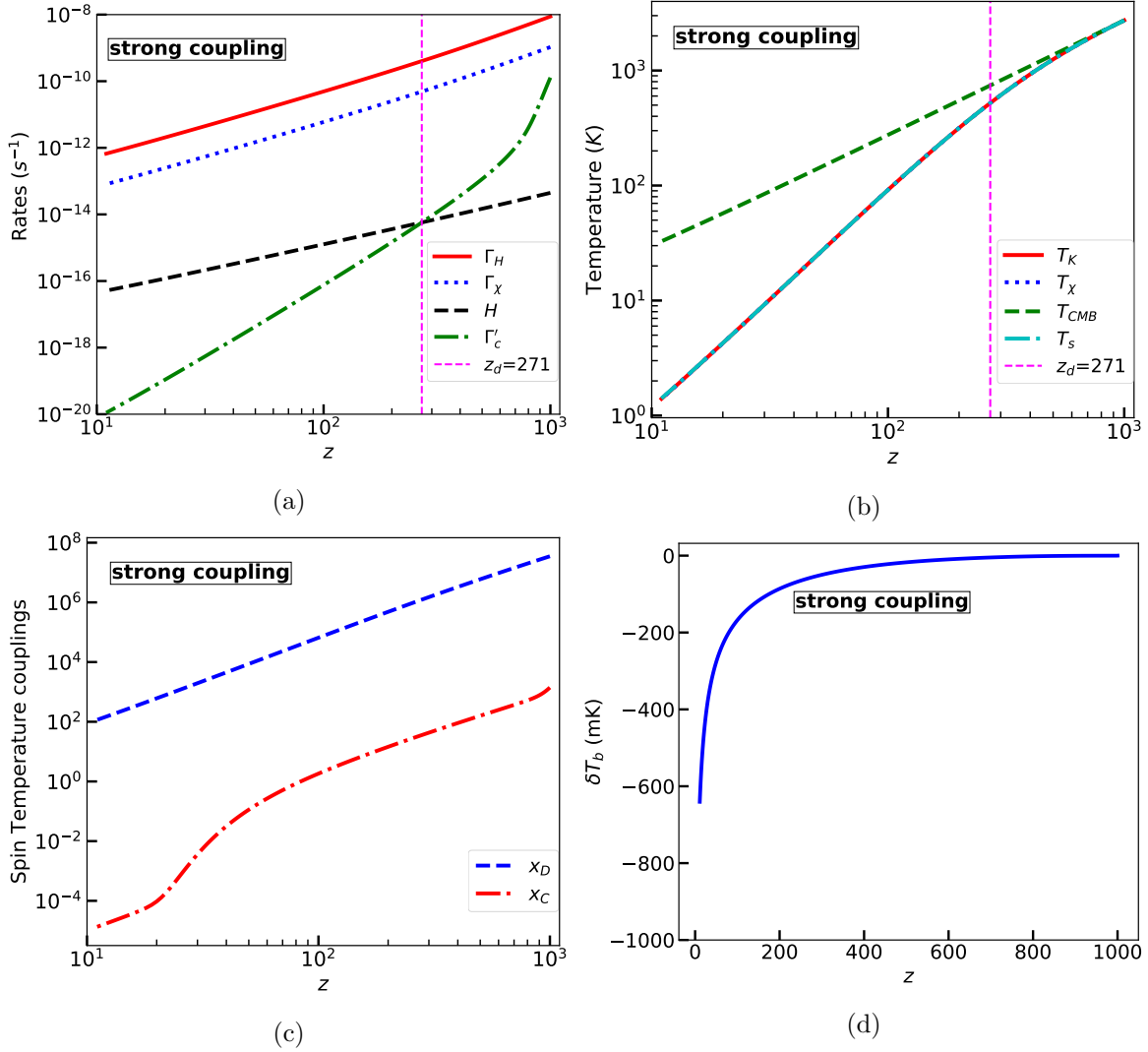
Figure 2: Benchmark plots for the strong coupling scenario with parameters $f = 0.1$, $m_\chi = 0.06$ GeV and $\alpha_e \alpha_\chi = 5 \times 10^{-15}$. (a) Rate evolution of the DM (Γ_χ) and gas (Γ_H) kinetic coupling to each other. Also shown is the effective rate of coupling of the combined DM-gas fluid to the CMB (Γ'_c) indicating a decoupling at $z = 271$. (b) Temperature evolution of the DM and gas kinetic temperatures, compared to the CMB temperature. The gas and DM are tightly kinetically coupled to each other and have a common temperature evolution. Adiabatic cooling of the tightly coupled DM-gas fluid begins at $z = 271$ and leads to a low $T_{\rm eff}$ at $z = 17$. The spin temperature is tightly coupled to the DM-gas temperature through a large spin-flip rate x_D. (c) The collisional coupling x_C to the gas kinetic temperature T_K, and the spin-flip coupling x_D to the effective temperature $T_{\rm eff}$. The DM induced spin-flip coupling rate dominates both the collisional and CMB induced spin-flip rates at all redshifts in this scenario. (d) Predicted differential brightness temperature $\delta T_b(z)$ as a function of redshift. The rise at low redshifts due to standard expected astrophysics is not shown.
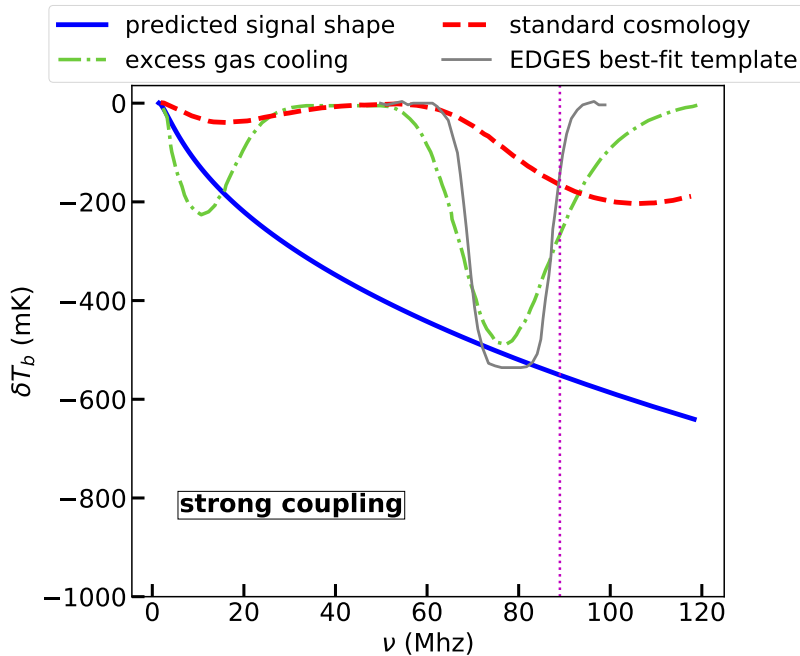
Figure 3: Predicted differential brightness temperature $\delta T_b(\nu)$ as a function of frequency (blue solid curve) with parameters $f = 0.1$, $m_\chi = 0.06$ GeV and $\alpha_e \alpha_\chi = 5 \times 10^{-15}$. Our model predicts a single, strong broadband absorption feature that begins at 5.3 MHz ($z = 271$) and extends all the way to high frequencies (~ 89 MHz ($z = 15$), indicated by the vertical dotted magenta line), with the expected rise at higher frequencies due to standard expected astrophysics not shown. We have also shown for comparison the prediction of the standard cosmology [18] (red dashed) and for an excess gas cooling model [60] (green dot-dashed) with parameters chosen to explain the EDGES absorption dip (gray) [33]. We see that, unlike our model, both these models have band-limited absorption features with transitions induced due to collisional couplings and Ly-α photons.

5.3 Scenario 2: Weak Coupling

5.3.1 Analytic understanding of weak coupling solutions

When the coupling product $\alpha_\chi \alpha_e$ is sufficiently weak, the DM and gas are kinetically decoupled from each other. In this scenario, the DM begins to cool adiabatically from the assumed initial condition, which is set at recombination. However, as we will show, for sufficiently low DM masses, *it is possible for the DM and gas to be kinetically decoupled (small Γ_χ), while still having a strong spin-flip interaction rate (large D_{10}).* The spin-flip rate of the gas due to DM interactions can be large enough so that the spin temperature couples to the cold dark matter temperature and we can get a large absorption dip in the differential brightness temperature in this scenario.

Since we have decided to anchor our absorption spectrum to a fixed value at $z = 17$, we are interested in looking for regions of parameter space that give rise to a large spin-flip rate at this particular redshift.

Assuming that $\Gamma_\chi \ll H$ at $z = 1000$, would guarantee decoupling of the DM from the gas. Since we have assumed the initial condition to be $T_\chi = T_K = T_{\text{CMB}}$ at $z = 1000$, we

would thus have the following temperature evolution of the DM temperature

$$T_\chi(z) = T_{\text{CMB}}(z = 1000) \left(\frac{1 + z}{1 + 1000} \right)^2 . \tag{5.10}$$

For small DM mass, $T_{\text{eff}}(z) \simeq T_\chi(z)$. At our anchor point $z = 17$, this would lead to $T_{\text{eff}}(z = 17) = 0.9$ K, which would be the coldest possible T_{eff} at this redshift, given our initial conditions.

The hierarchy between the DM induced spin-flip rate of neutral hydrogen (D_{10}) and the kinetic coupling rate of DM to the gas (Γ_χ) is possible because $\Gamma_\chi = \frac{3S}{R} D_{10}$, where $S = \left(\frac{\Delta \mu}{2MT_{\text{eff}}} \right) \ll 1$, and $R = \frac{n_\chi}{n_H} \gg 1$, for sufficiently low DM masses (see discussion following eq. 4.6). In particular, given the scaling of T_{eff} as $(1 + z)^2$, we can see that $D_{10} \propto \frac{1}{m^{3/2}} (1 + z)^4$ (see eq. 3.13) and $\Gamma_\chi \propto m^{1/2} (1 + z)^2$ (see eq. 4.6). Thus, although D_{10} drops rapidly with redshift, for sufficiently low DM masses it is still possible to obtain a large spin-flip rate $D_{10} \sim B_{10}$ at $z = 17$, while insisting that the DM decouples at $z = 1000$, $H \gg \Gamma_\chi$ at $z = 1000$.

Since we have assumed that Ly-α couplings have not yet turned on at $z = 17$, and also since the collisional couplings can be neglected at this redshift, we have,

$$T_s^{-1} \simeq \frac{T_{\text{CMB}}^{-1} + x_D T_{\text{eff}}^{-1}}{1 + x_D} . \tag{5.11}$$

In order to obtain $\delta T_b(z = 17) = -500$ mK, we would need $T_s(z = 17) \simeq 3.32$ K. Plugging this desired value into the left-hand side of the equation above, and for the lowest possible value of $T_{\text{eff}} = 0.9$ K at $z = 17$, this would imply that we need $x_D(z = 17) = 0.34$, i.e. $D_{10} = 0.34 B_{10}$; moderate, but not tight spin-flip coupling at $z = 17$ is needed since T_{eff} is much colder than the desired spin temperature[4].

This condition on x_D gives us,

1. Criteria for moderate spin-flip coupling $\mathbf{x_D(z = 17) = 0.34}$:

$$\alpha_e \alpha_\chi = \frac{5.6 \times 10^{-17}}{f} \left(\frac{m_\chi}{\text{GeV}} \right)^{3/2} . \tag{5.12}$$

For self-consistency of our solution, we need the coupling to be sufficiently weak so that we are in the regime where the DM decouples at $z = 1000$, this criteria is given by the requirement that $\Gamma_\chi \lesssim H/10$ at $z = 1000$, or in terms of the couplings,

2. Self-consistency criteria for weak kinetic coupling of DM:

$$\alpha_e \alpha_\chi < 5.1 \times 10^{-21} \sqrt{\frac{\text{GeV}}{m_\chi}} . \tag{5.13}$$

Comparing this with criteria 1 above, we see that our weak coupling solution is valid only up to a maximum mass (or maximum coupling). We can thus write down criteria 2 in the form below,

2′. Modified self-consistency criteria for weak kinetic coupling of DM:

$$m_\chi < 9.5 \times 10^{-3} \sqrt{f} \text{ GeV}, \tag{5.14}$$

---

[4]For the range of -600 mK $< \delta T_b(z = 17) < -400$ mK or 2.7 K $< T_s(z = 17) < 3.9$ K, we need $0.27 < x_D(z = 17) < 0.47$. In our numerical scan, we take the criteria $x_D(z = 17) < 0.47$ to define the weak coupling regime of the parameter space.

or equivalently,

$$\alpha_e \alpha_\chi < \frac{5.2 \times 10^{-20}}{f^{1/4}}. \tag{5.15}$$

These two criteria 1 and 2 (or 2′) give us an analytic range of parameters m_χ and $\alpha_\chi \alpha_e$ for a given value of f, which define the weak coupling region of our parameter space. We have plotted this analytic solution in each of the panels of fig. 1.

What happens to the baryons in this scenario?
There are two possible histories for the baryonic temperature evolution which depend upon the mass of the DM particle in our parameter space of interest. We will discuss each of these possibilities in turn.

Possibility 1: No excess cooling as compared to the standard cosmology for very low DM masses
If $\Gamma_H < H$ at $z = 1000$, the gas will just decouple from the DM and cool at $z = 130$ adiabatically as in the standard scenario with no exotic DM couplings. This criteria can be reexpressed as,

$$\alpha_e \alpha_\chi < \frac{9.9 \times 10^{-21}}{f} \left(\frac{m_\chi}{\text{GeV}} \right)^{1/2}. \tag{5.16}$$

This condition is satisfied for parameters that satisfy criteria 1, as long as $m_\chi < 1.8 \times 10^{-4}$ GeV. For such low values of DM mass, the baryon temperature evolution is completely unaffected and the gas kinetic temperature would be large compared to the spin temperature, i.e. the gas would have a temperature $T_K(z = 17) = 6.8$ K, as in the standard cosmology without exotic DM interactions, whereas the spin temperature $T_s(z = 17) = 3.32$ K. Despite the large gas *kinetic* temperature, the gas *spin* temperature is low enough to lead to a strong absorption signal at $z = 17$ because of a combination of the large DM spin-flip rate D_{10} at $z = 17$ and the low DM temperature.

Possibility 2: Super-adiabatic cooling
For larger values of the dark matter mass, 1.8×10^{-4} GeV $< m_\chi < 9.5 \times 10^{-3}\sqrt{f}$ GeV[5], the baryons have two competing rates which determine their temperature evolution, on the one hand the coupling to DM which tries to lower the baryon temperature, and the coupling to CMB which tries to keep the baryons at the CMB temperature. $\Gamma_H \propto (1 + z)^2$ and $\Gamma_c \propto (1 + z)^4 x_e(z)$, so at some point it is conceivable that if the coupling is not too small, Γ_H can become the dominant rate that determines the evolution of the gas temperature. If $\Gamma_H > H$, the gas will cool *super-adiabatically* (faster than $(1 + z)^2$) in a bid to latch on to the low DM temperature. If at some redshift $\Gamma_H < H$, then the gas will switch to cooling adiabatically from this point onwards with $T_K \propto (1+z)^2$. In general, the evolution of the gas temperature in this range of DM masses is complicated and must be solved for numerically.

Note that for both possibilities in the weak coupling scenario, the evolution of the gas temperature is practically irrelevant for (and distinct from) the evolution of its spin temperature (since $T_{\text{eff}} \sim T_\chi$ for low DM masses), as long as the coupling x_D is the dominant spin-flip coupling. *The absorption signal in this scenario would trace only the spin-temperature and not the kinetic temperature of the gas for most of the cosmological history, as opposed to the*

---

[5]This range exists for all the benchmark values of f that we are considering. For smaller values of f this interval shrinks to zero size, and this second type of weak coupling solution does not exist; the baryons would just cool as in the standard cosmology.

standard cosmology or even excess gas cooling models where the absorption signal is expected to be a tracer of the gas kinetic temperature. At low redshifts, if Ly-α coupling becomes strong due to star formation, then the gas temperature becomes relevant for determining the further evolution of the spin temperature and hence could be tracked using the differential brightness temperature.

5.3.2 Numerical results for weak coupling benchmark point

In our numerical scan, we identify the weak coupling regions of our parameter space by the criteria $x_D(z = 17) < 0.47$. We will discuss a particular benchmark point with $f = 0.1$, $m_\chi = 1.1 \times 10^{-3}$ GeV and $\alpha_e \alpha_\chi = 2.7 \times 10^{-20}$. This benchmark point satisfies the criteria of moderate spin-flip coupling in eq. 5.12 and also the mass lies in the relatively larger range for this scenario, 1.8×10^{-4} GeV $< m_\chi < 9.5 \times 10^{-3}\sqrt{f}$ GeV.

In fig. 4a, we show the reaction rates Γ_H, Γ_χ, Γ_c and the Hubble rate H as functions of z for this benchmark point. We can see from the figure that the rate Γ_χ is less than the Hubble rate throughout the redshift range $10 \lesssim z \lesssim 1000$, indicating that the DM decouples from the gas (and the CMB) and begins cooling adiabatically from the initial condition assumed at $z = 1000$. Meanwhile, the rate Γ_H is larger than the Hubble rate throughout the redshift range $10 \lesssim z \lesssim 1000$, indicating that the gas is kinetically coupled to the adiabatically cooling DM. However, the gas is also coupled to the CMB and at high redshifts, and it is this interaction which dominantly determines the evolution of the gas kinetic temperature at early times.

The evolution of the gas and DM kinetic temperatures are shown in fig. 4b. At low DM masses, as at this benchmark point, the effective temperature $T_{\text{eff}} \simeq T_\chi$, and since the DM is cooling adiabatically, T_{eff} cools as $(1 + z)^2$. At $z = 17$, $T_{\text{eff}} \simeq 0.9$ K, which is the coldest possible value for the effective temperature. The gas is initially tightly coupled to the CMB and tracks the CMB temperature from $z \sim 1000$ down to $z \sim 300$. Near $z \sim 300$, the kinetic coupling of the gas to the CMB and the coupling of the gas to the DM become comparable, indicating a competition between these two rates in determining the evolution of T_K. The coupling to the DM makes the gas cool below the CMB temperature. Finally, at low redshifts ($z \lesssim 200$), the only relevant coupling is of the gas to the DM, and the gas attempts to cool super-adiabatically down to the DM temperature.

In fig. 4c, we show the evolution of the spin-temperature coupling (x_D) to the temperature T_{eff}, and the collisional coupling (x_C) to the gas temperature T_K. At all redshifts, we see that the coupling $x_D \gg x_C$, which indicates that the DM spin-flip coupling reaction rate D_{10} dominates over the collisional coupling rate. Moreover, from $40 \lesssim z \lesssim 1000$, $x_D \gtrsim 1$, which implies that the DM spin-flip rate D_{10} is larger than the CMB induced spin-flip rate B_{10} over this redshift range. Thus, the spin temperature T_s is tightly coupled to T_{eff} from $z \sim 1000$ till a redshift $z \sim 40$. At $z \sim 40$, $x_D \sim 1$ and the CMB induced spin-flip rate B_{10} begins to compete with the DM induced spin-flip rate D_{10}. We can see this behaviour in the evolution of T_s shown in fig. 4b. T_s initially tracks the dark matter temperature till $z \sim 40$, but then as the coupling x_D drops to $\mathcal{O}(1)$ values, the spin temperature begins to cool slower than the adiabatically cooling DM and eventually attempts to rise back up towards the CMB temperature. For the benchmark set of parameters we have chosen, $T_s = 2.8$ K at $z = 17$ – a value which is intermediate between the DM temperature of 0.9 K and the CMB temperature of 49 K at this redshift.

In fig. 4d, we show the differential brightness temperature as a function of redshift z, inferred from the spin temperature evolution history. Since $\delta T_b \propto T_s - T_{\text{CMB}}$ and T_s drops and

stays below T_{CMB} at high redshifts (from $40 \lesssim z \lesssim 1000$), we see a dip in δT_b which begins at our initial conditions of $z \sim 1000$. We get a minimum of δT_b at $z = 40$, where $x_D \sim 5$. As the coupling x_D drops further from this point onwards, the spin temperature attempts to rise back up to the CMB temperature, we get a rise in δT_b till lower redshifts. Since $T_s = 2.8~K$ at $z = 17$, this leads to a differential brightness temperature dip $\delta T_b(z = 17) \simeq -580$ mK.

In this scenario, we see that it is possible to get *both a dip and a rise* in the differential brightness temperature, purely from a combination of the DM temperature evolution and the spin-flip coupling x_D, *even without considering Ly-α couplings.* However, we expect that below some redshift, $z \lesssim 15$, Ly-α coupling to T_K would turn on due to star formation, and X-ray heating would raise T_K. Since the details of this would depend on the astrophysical model we do not show the effects of this in our figure.

In fig. 5, we show the differential brightness temperature evolution as a function of redshifted 21 cm frequency. We also show for comparison, in the same figure, the expected band-limited signals from the standard cosmology and from the excess gas cooling model of [60]. Once, again we see in our model a prediction of a single, strong, broadband absorption feature which extends from $\nu = 1.4$ MHz $(z = 1000)$[6] all the way up to $\nu = 89$ MHz $(z = 15)$, unlike the two distinct band-limited absorption features of the standard cosmology and excess cooling models. The key observational feature of the weak coupling absorption spectrum that distinguishes it from the strong coupling scenario, is the existence of a deep minimum of δT_b at low frequencies originating from the cosmic dark ages – near 35 MHz $(z = 40)$ for our benchmark point. From this point onwards, δT_b rises up and at 78 MHz $(z = 17)$, the spectrum reaches its "pinned" value of $\delta T_b \simeq -580$ mK.

Above 89 MHz $(z = 15)$, Ly-α photons and X-ray heating could lead to two distinct possibilities: a) if X-ray heating is rapid and precedes strong Ly-α coupling, then the gas temperature would quickly rise up towards the CMB temperature, and the spin temperature would later attempt to latch on to this large T_K. In this case, the rise in δT_b at higher frequencies would continue at a rate faster than what is shown in the figure, b) if strong Ly-α coupling turns on before X-ray heating, then the spin-temperature would attempt to cool again to the low gas temperature, leading to a second, relatively weaker dip in the absorption spectrum before rising again. Unlike the excess cooling models, this second dip would be less well separated from the broadband signal. Since, the details of these high frequency features depend on the astrophysical model, we have not shown them in our figure.

---

[6]This value depends on our assumed initial conditions, since we assumed $T_\chi = T_{\mathrm{CMB}}$ at $z = 1000$, no absorption is expected at higher redshifts/lower frequencies.
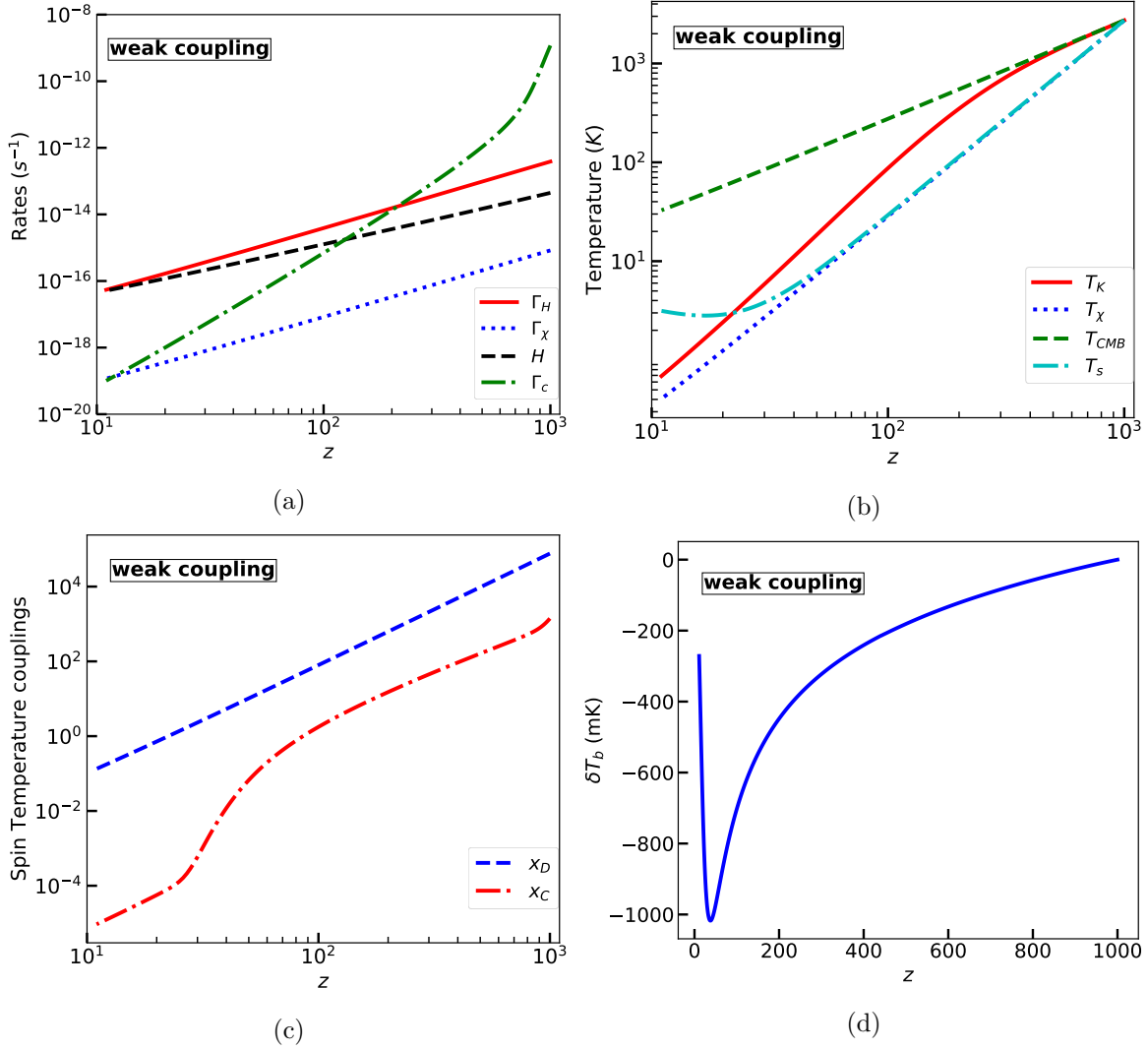
Figure 4: Benchmark plots for the weak coupling scenario with parameters $f = 0.1$, $m_\chi = 1.1 \times 10^{-3}$ GeV and $\alpha_e \alpha_\chi = 2.7 \times 10^{-20}$. (a) Rate evolution of the DM (Γ_χ) and gas (Γ_H) kinetic coupling to each other and the rate coupling Γ_c of the gas to the CMB. For this scenario, the dark matter is decoupled from both the gas and the CMB, and adiabatically cools from our initial conditions at $z = 1000$. (b) Temperature evolution of the DM and gas kinetic temperatures compared to the CMB temperature. The effective temperature is given by $T_{\text{eff}} \simeq T_\chi$ for low DM masses. The spin temperature T_s is initially tightly coupled to T_{eff} through a large spin-flip coupling rate x_D, but then starts to heat up to the CMB temperature at $z \sim 40$, when $x_D \sim 5$. The gas kinetic temperature and the spin temperature evolve almost completely independently in this scenario. (c) The collisional coupling x_C to the gas kinetic temperature T_K and the spin-flip coupling x_D to the effective temperature T_{eff}. The rate D_{10} dominates over both the collisional and the CMB spin-flip rates till $z \sim 40$, but below this redshift the coupling of T_s to the CMB temperature begins to dominate and the spin temperature attempts to rise towards T_{CMB}. (d) Predicted differential brightness temperature $\delta T_b(z)$ as a function of redshift. The low redshift behavior ($z \lesssim 15$) due to the astrophysics of Ly-α coupling and X-ray heating is not included in the figure.
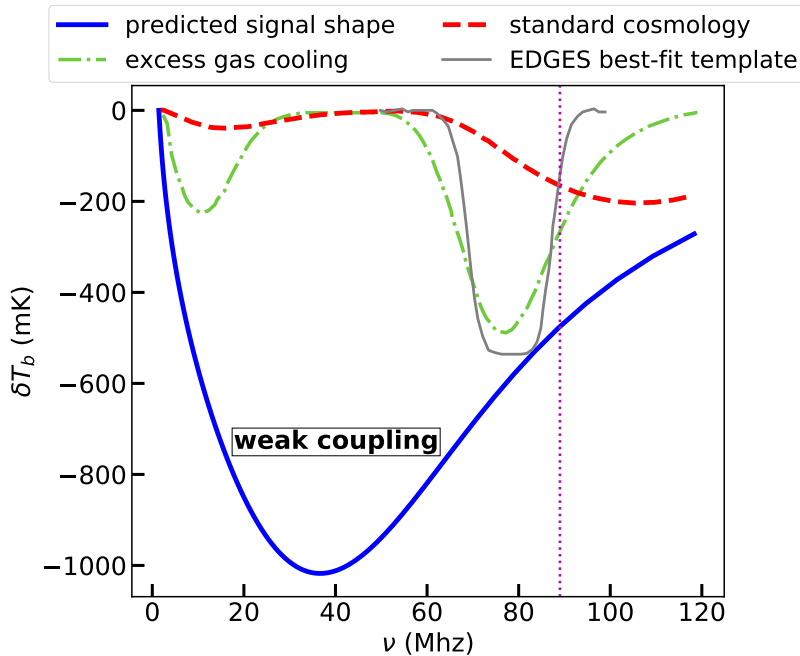
Figure 5: Predicted differential brightness temperature $\delta T_b(\nu)$ as a function of frequency (blue solid curve) with parameters $f = 0.1$, $m_\chi = 1.1 \times 10^{-3}$ GeV and $\alpha_e \alpha_\chi = 2.7 \times 10^{-20}$. Our model predicts a single, strong broadband absorption feature that begins at 1.4 MHz ($z \sim 1000$) and extends all the way to high frequencies (~ 89 MHz ($z \sim 15$), indicated by the vertical dotted magenta line). Unlike the strong coupling scenario, in this scenario we get a deep minima from the cosmic dark ages at 35 MHz, ($z \simeq 40$), as the spin temperature attempts to rise up towards the CMB temperature. At frequencies above 89 MHz, Ly-α couplings and X-ray heating could lead either to a sharper rise or a possible second dip, but these features are not shown in the figure. Unlike our model where the absorption feature is due to DM spin-flip interactions, both the standard cosmology (red dashed) and excess gas cooling models (green dot-dashed) have distinct band-limited absorption features with transitions due to collisional couplings and Ly-α photons.

5.4   Scenario 3: Intermediate Coupling

5.4.1   Qualitative understanding of intermediate coupling solutions

This scenario, as the name suggests, lies between the scenarios of strong and weak coupling. In this scenario, the gas and dark matter are initially tightly kinetically coupled to each other (similar to the strong coupling scenario), but as they evolve, they might either cool together adiabatically, or the dark matter might decouple from the baryons and begin to cool adiabatically on its own. In either case, the effective temperature T_{eff} at $z = 17$ is less than the desired spin temperature of 3.32 K, as required by our pinning of the absorption spectrum. With moderate values of the spin-flip coupling (similar to the weak coupling scenario) it is possible to obtain $T_s(z = 17) \simeq 3.32$ K, and thus, $\delta T_b(z = 17) = -500$ mK.

The intermediate coupling parameter space can be further subdivided into two distinct behaviors at larger and smaller couplings which we discuss below.

For larger couplings in the intermediate region, the DM and the gas remain tightly

coupled throughout their evolution, which is similar to the tight kinetic coupling of the strong coupling scenario. However, the DM masses are slightly lower than $m_\chi \lesssim 0.68 f$ (see discussion of scenario 1 on criteria needed for decoupling of the combined gas-DM system from the CMB and eq. 5.5). This implies that $R = \frac{n_\chi}{n_H} > 7.6$, which in turn implies that the effective coupling rate of the gas-DM fluid to the CMB, $\Gamma'_c = \frac{1}{1+R}\Gamma_c$, is weaker than in scenario 1 and thus the combined fluid decouples *earlier* than $z = 265$, i.e. between $z = 1000$ and $z = 265$. This leads to an effective temperature $T_{\rm eff}(z = 17)$ that is *lower* than the value of 3.32 K, which is our desired value of the spin-temperature T_s at $z = 17$. We can still obtain the desired T_s value at $z = 17$ for low $T_{\rm eff}$, if the spin-flip coupling x_D is low enough so that the coupling rates of the spin temperature to $T_{\rm CMB}$ (B_{10}) and to $T_{\rm eff}$ (D_{10}) are comparable. In this respect, the situation is similar to the weak coupling scenario with respect to moderate spin-flip couplings.

For smaller couplings in the intermediate region, the DM is initially tightly coupled to the gas (and in this way the scenario is distinct from the weak kinetic coupling of scenario 2), but it may decouple earlier than $z = 265$. However, for low DM masses, $T_{\rm eff}$ is once again dominated by T_χ and the spin temperature couples to the cold dark matter kinetic temperature. In this case, as in the weak coupling scenario, for moderate values of the spin-flip coupling x_D, it is possible to obtain $T_s = 3.32$ K. The baryons continue to be tightly kinetically coupled to the DM, since $\Gamma_H = R\Gamma_\chi$ and $R > 1$, and eventually once the kinetic coupling to the CMB becomes irrelevant, they cool super adiabatically towards the DM temperature. This regime is very similar to the behavior of the weak coupling scenario except for the initial tight coupling of the DM to the gas, which leads to a slightly hotter $T_{\rm eff}$ (or T_χ) at $z = 17$, than in the weak coupling scenario.

In either situation, of relatively larger or smaller coupling, $T_{\rm eff}$ is lower than 3.32 K at $z = 17$ for all benchmark points in the intermediate scenario. At the redshift where $x_D \sim 1$, we get a switch in the behaviour of T_s from tracking $T_{\rm eff}$ towards attempting to track the CMB temperature. Near the redshift where $x_D \sim 1$, the differential brightness temperature δT_b is at its minimum. In the intermediate coupling regime it is possible to find points in parameter space where not only is the spin temperature $T_s(z = 17) \simeq 3.32$ K, thus giving us the desired magnitude of the absorption dip in the brightness temperature at 78 MHz, but it is also possible to find a point among these, where $z = 17$ ($\nu = 78$ MHz) is also a *minimum* of the differential brightness temperature. We will discuss such a benchmark point in the next subsection.

We note that like the weak coupling scenario, even in the intermediate coupling regime, the absorption signal is only a tracer of the spin temperature, which can differ from the gas kinetic temperature. The deviation between the T_s and T_K is most significant as we go towards the region of parameter space with smaller couplings. However, for couplings near the upper end of the intermediate coupling regime (including at our benchmark point), the deviation between the spin temperature and the kinetic temperature of the gas is only significant over a small redshift range prior to the cosmic dawn.

5.4.2 Numerical results for intermediate coupling benchmark point

In our numerical scan, we identify the region in parameter space for this scenario by demanding that $0.47 \lesssim x_D \lesssim 10$ at $z = 17$. Now we discuss a particular benchmark point with $f = 0.1$, $m_\chi = 0.05$ GeV and $\alpha_e \alpha_\chi = 4.3 \times 10^{-17}$. This point is in the relatively more strongly coupled regime of the intermediate coupling scenario.

In fig. 6a, we show the reaction rates Γ_H, Γ_χ and the Hubble rate H as functions of z for this benchmark point. We can see from the figure that the rates Γ_χ and Γ_H are larger than the Hubble rate throughout the redshift range $10 \lesssim z \lesssim 1000$, indicating that the DM and the gas are tightly coupled to each other, as in the strong coupling scenario. This behaviour is clearly seen in fig. 6b, in which we show the temperature evolution of T_K and T_χ, where both temperatures track each other very closely. In fig. 6a, we also plot the effective "compton coupling rate" of the DM-gas fluid to the CMB Γ'_c, and we see that this rate decouples (drops below the Hubble rate) at $z = 290$. In fig. 6b, we can see the common temperature evolution of the DM-gas switches from tracking the CMB temperature (and scaling as $(1 + z)$) from $z = 1000$ till $z = 290$, to adiabatic cooling (scaling as $(1 + z)^2$) from $z = 290$ onwards to lower redshifts.

In fig. 6c, we show the evolution of the spin-temperature coupling x_D to the temperature T_{eff} (which is just the same as the common temperature of the gas-DM fluid for strong kinetic coupling), and the collisional coupling x_C to the gas temperature T_K. At all redshifts from $25 \lesssim z \lesssim 1000$, we see that the coupling $x_D \gg x_C$, which indicates that the DM spin-flip coupling reaction rate D_{10} is dominant over the collisional coupling spin-flip rate. However, at $z = 25$, $x_D = 13 \sim \mathcal{O}(10)$ and the CMB induced spin-flip rate B_{10} becomes comparable to the rate D_{10} of DM induced spin-flip interactions. Thus, over the redshift range $25 \lesssim z \lesssim 1000$, T_s tracks the common temperature of the gas-DM fluid. However, at $z \sim 25$, the spin-temperature begins heating up towards the CMB temperature (or at least cools more slowly than the adiabatically cooling DM-gas fluid). The evolution of the spin-temperature of the gas is shown in fig. 6b. We can see that this scenario is intermediate between scenario 1 (strong coupling) and scenario 2 (weak coupling), in that while the DM and gas are tightly kinetically coupled to each other (as in scenario 1), the DM induced spin-flip rate drops below (or becomes comparable to) the CMB induced spin-flip rate at low redshifts (as in scenario 2).

The early decoupling of the gas-DM fluid at $z = 290$ leads to a value of $T_{\text{eff}} = 2.9$ K at $z = 17$. This combined with the moderate spin-flip coupling $x_D(z = 17) = 4.5$, leads to a spin temperature $T_s(z = 17) = 3.5$ K, intermediate between T_{eff} and the CMB temperature at this redshift. This can be seen in fig. 6b, where we have also plotted the evolution of the spin temperature with redshift.

In fig. 6d, we show the differential brightness temperature as a function of redshift z, inferred from the spin temperature evolution history. Since, $\delta T_b \propto T_s - T_{\text{CMB}}$ and T_s drops faster than T_{CMB} at high redshifts, we see that δT_b becomes more negative as we go from a redshift of $z \sim 1000$ to $z \sim 25$. From this point on, the spin temperature begins to heat up towards the CMB temperature. Thus, we expect δT_b to attain a minimum for some lower redshift. For our particular benchmark point δT_b is at a minimum at $z = 17$. Also, as for all points in our parameter space of interest, the low spin temperature leads to a dip in $\delta T_b(z = 17) \simeq -457$ mK, near our "pinned" value.

Once again, we expect that below some redshift $z \lesssim 15$, Ly-α coupling to T_K would turn on due to star formation, and X-ray heating would raise T_K, altering the behavior of the differential brightness temperature for lower redshifts. However, since the details of this would depend on the astrophysical model, we do not show these effects in our figure.

In fig. 7, we show the differential brightness temperature evolution as a function of redshifted 21 cm frequency. We also show for comparison, in the same figure, the expected distinct band-limited signals from the standard cosmology and in the excess gas cooling model of [60]. Again, we see the contrast between these signals, and our model which predicts a

single, strong, broadband absorption feature that extends from 4.9 MHz ($z = 290$) all the way up to 89 MHz ($z = 15$). At 78 MHz ($z = 17$), the spectrum in our model attains the "pinned" value of $\delta T_b \simeq -457$ mK. The minima of the absorption spectrum for this benchmark point is also at 78 MHz, a frequency value which is intermediate between the weak coupling minima at 35 MHz and the strong coupling minima at $\nu > 89$ MHz, (compare fig. 7 with figs. 5 and 3).

For frequencies larger than 89 MHz, Ly-α photons from the first stars and X-ray heating would determine the behavior of the absorption spectrum. Depending upon the time order in which these effects come into play, we could either get a sharp rise in the predicted spectrum above 89 MHz, or a possible second dip before the rise. In the latter case, unlike the excess cooling models, the second absorption dip would be less well separated from the first absorption dip in the broadband signal. Since the details depend on the astrophysical model, we have not shown these possible effects in the figure.
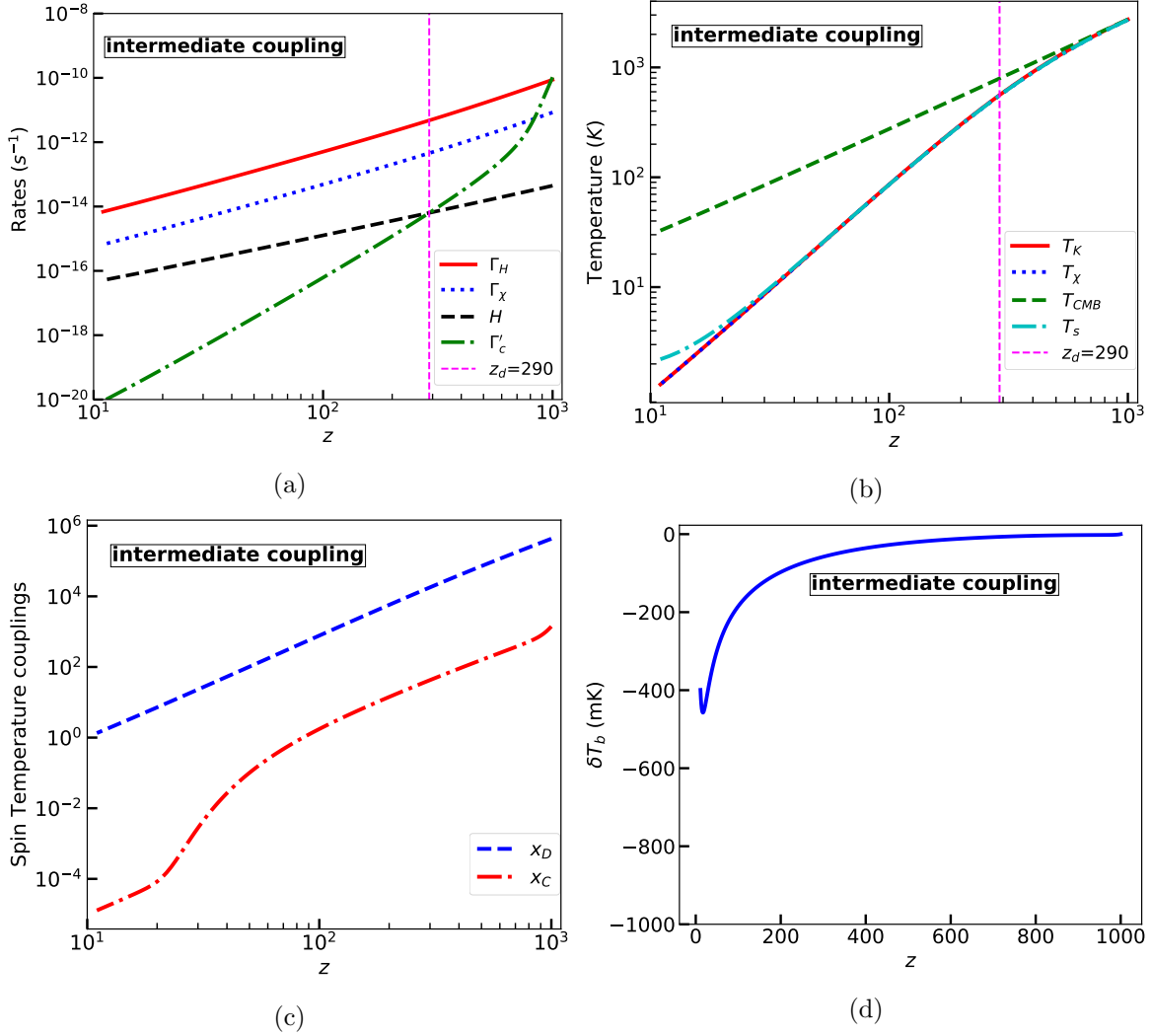
Figure 6: Benchmark plots for the intermediate coupling scenario with parameters $f = 0.1$, $m_\chi = 2.5 \times 10^{-2}$ GeV and $\alpha_e \alpha_\chi = 1.1 \times 10^{-17}$. (a) Rate evolution of the DM (Γ_χ) and gas (Γ_H) kinetic coupling to each other and the effective coupling of the combined DM-gas fluid to the CMB (Γ'_c) indicating a decoupling at $z = 290$. (b) Temperature evolution of the DM and gas kinetic temperatures compared to the CMB temperature. Adiabatic cooling begins at $z = 290$ and leads to $T_{\rm eff} = 2.9$ K at $z = 17$. The spin temperature is tightly coupled to the DM-gas temperature through a large spin-flip rate x_D at high redshifts, but at redshifts below $z \sim 25$, the spin temperature is also heated up by the CMB temperature (away from $T_{\rm eff}$) as x_D drops below ~ 10 (c) The collisional coupling x_C to the gas kinetic temperature T_K and the spin-flip coupling x_D to the effective temperature $T_{\rm eff}$. The rate D_{10} dominates over both the collisional rate and the CMB rate till $z \sim 25$, but for lower redshifts the coupling of T_s to the CMB temperature begins to dominate and the spin temperature rises (or falls slower than the temperature of the adiabatically cooling DM-gas fluid). (d) Predicted differential brightness temperature $\delta T_b(z)$ as a function of redshift. Additional contributions from astrophysics at low redshifts $z \lesssim 15$ are not shown.
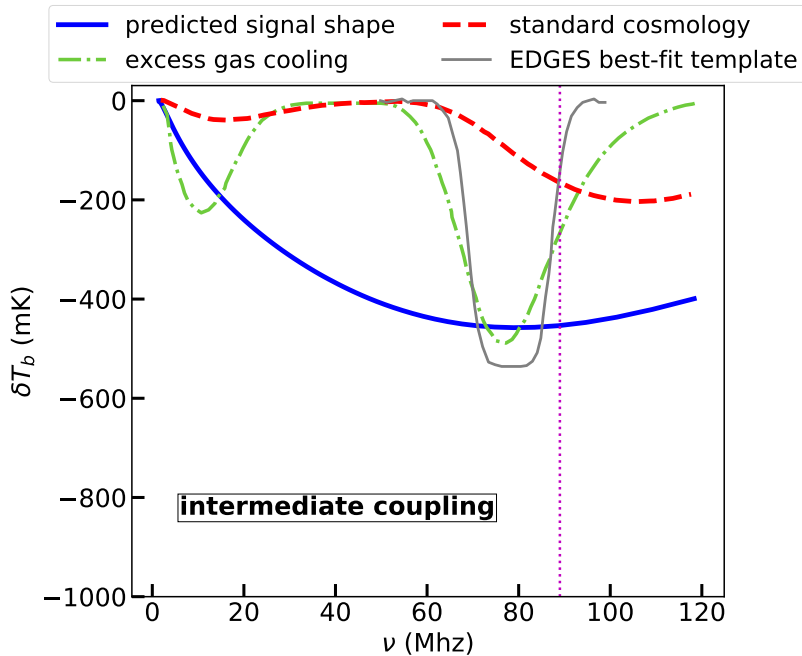
Figure 7: Predicted differential brightness temperature $\delta T_b(\nu)$ as a function of frequency (blue solid curve) with parameters $f = 0.1$, $m_\chi = 2.5 \times 10^{-2}$ GeV and $\alpha_e \alpha_\chi = 1.1 \times 10^{-17}$. Our model predicts a single, strong broadband absorption feature that begins at 4.9 MHz ($z = 290$) and extends all the way to high frequencies (~ 89 MHz ($z = 15$), indicated by the vertical dotted magenta line). For this particular benchmark point we get a minima at 78 MHz ($z = 17$) with a value $\delta T_b(\nu = 78$ MHz$) \simeq -457$ mK. The minima arises as the spin temperature attempts to rise up towards the CMB temperature. Above 89 MHz, Ly-α couplings and X-ray heating could lead to either a sharper rise or a possible second dip, but these features are not shown. Unlike our model, both the standard cosmology (red dashed) and excess gas cooling models (green dot-dashed) have band-limited absorption features with transitions due to collisional couplings and Ly-α photons.

5.5 Summary of the absorption signal expected in different regions of the parameter space

We have seen that in all scenarios, our model predicts a single, strong broadband absorption signal starting from early in the cosmic dark ages. This signal is unlike the two distinct band-limited absorption features expected in the standard cosmology and excess gas cooling models. In any of the panels in fig. 1, we can imagine following a curve through the parameter space of interest starting at strong coupling and proceeding through intermediate coupling, on to weak coupling. The predicted absorption spectra as we follow this curve can be tracked by comparing figs. 3, 7, 5 in order. In all cases, by our benchmark choice, our predicted absorption spectrum is pinned at 78 MHz, to have a value $\delta T_b \simeq -500$ mK. However, as we go from strong coupling to intermediate coupling to weak coupling, the minima of the absorption signal shifts from frequencies greater than 89 MHz at strong coupling, to ~ 78 MHz at intermediate coupling, to even lower frequencies at weak coupling. In the latter two scenarios, it is possible that there might be a second absorption dip at frequencies > 89 MHz

due to Ly-α photons and X-ray heating, which is not well separated from the broadband signal which is due to the DM spin-flip coupling. The start of the absorption dip also drifts slightly to lower frequencies, starting at 5.3 MHz for the strong coupling scenario, moving to 1.3 MHz for the weak coupling scenario. This low frequency region is a regime of frequencies from which no signal is expected at all in the standard cosmology or in excess cooling models.

Another prediction which is in stark contrast to the expectation of the standard cosmology or excess cooling models, is that our predicted absorption signal is a tracer of the gas spin temperature and not necessarily of the gas kinetic temperature. In the weak and intermediate coupling scenarios, we have seen that the strong spin-flip coupling would relate T_s to $T_{\text{eff}} \simeq T_\chi$, but the weak kinetic coupling in these regions of parameter space will not allow the gas kinetic temperature T_K to cool down to T_χ.

What would happen to our predicted signal if we move slightly away from the benchmark parameter space shown in fig. 1? We can imagine following a contour parallel to our parameter space towards the upper left (smaller m_χ near strong coupling, and larger couplings for a given m_χ near weak coupling). From our discussion of the analytic predictions of the spin temperature, it is easy to see that such a change would lead to a stronger benchmark absorption signal at $z = 17$, thus altering our pinning point. Similarly, if we shift our preferred parameter space to the lower right, this would lead to a weaker absorption signal at $z = 17$. For such small deviations in the parameter space, the shape of the signal would remain mostly unaltered. However, for larger variations across the parameter space, especially towards weaker coupling, we would expect to see significantly different behavior in the predicted absorption signal, as the coupling x_D becomes small enough that the collisional coupling of the spin temperature to the gas kinetic temperature becomes cosmologically relevant once again.

6 Some clarifications about assumptions

6.1 Initial conditions

Now we discuss the choice of initial conditions that we had assumed for solving the temperature evolution equations. Our default choice was to choose our initial conditions near recombination, and we assumed $T_\chi = T_K = T_{\text{CMB}}$ at $z = 1000$.

The pre-recombination behavior that determines the initial conditions depends on the thermal history of the DM particle and the dark sector in general. The initial conditions are therefore model dependent, because interactions of the DM other than the spin-flip interactions considered here are also important for determining the kinetic coupling of the DM to either the visible sector plasma or a possible dark radiation bath.

However in all models, the spin-flip interaction with electrons that we have considered would lead to a minimum level of elastic scattering between DM and electrons, which can kinetically couple the DM to the visible sector plasma in the pre-recombination era. The energy transfer cross-section for DM-electron scattering is of the form (see appendix B),

$$\overline{\sigma}_{e\chi} = \frac{3}{8\pi} \frac{g_\chi^2 g_e^2}{\mu_{\chi e}^2 v^4} \text{Log}\left(\frac{4\mu_{\chi e}^2 v^2}{m_V^2}\right), \tag{6.1}$$

where $\mu_{e\chi}$ is the reduced mass of the dark matter and electron and v is the relative velocity between the incoming DM and the electron. From this we can estimate the energy transfer

rate coefficient from the electrons to DM as,

$$\Gamma_\chi^e \sim n_e \frac{3}{8\pi} \frac{g_\chi^2 g_e^2}{T_{\text{eff}}^2} \left(\frac{\mu_{e\chi}}{M_{e\chi}} \right) \text{Log} \left(\frac{4\mu_{e\chi} T_{\text{eff}}}{2m_V^2} \right) \tag{6.2}$$

where $M_{e\chi}$ is the sum of the DM and electron masses, and we have estimated the thermal average cross-section by substituting $\mu_{e\chi} v^2 \to T_{\text{eff}}$, where $T_{\text{eff}} = \mu_{e\chi} \left(\frac{T_\chi}{m_\chi} + \frac{T_e}{m_e} \right)$, and T_e is the electron/visible sector plasma temperature. We have also included an additional suppression factor of $\frac{\mu_{e\chi}}{M_{e\chi}}$ expected for energy transfer between particles of unequal masses.

This energy transfer rate is log enhanced because the forward scattering divergence of the elastic scattering is cut-off by the small mediator mass m_V (rather than the mass splitting parameter Δ of inelastic scattering of DM with hydrogen). The energy transfer rate of inelastic scattering of DM with neutral hydrogen (Γ_χ) in the post-recombination era scales as $\frac{1}{T_{\text{eff}}\Delta}$ (see eq. A.60 in appendix A.3), since the forward scattering divergence is cut-off by the inelasticity parameter. Thus, we see that the pre-recombination energy transfer rate, Γ_χ^e has a net suppression by a factor of $\sim \frac{\Delta}{T_{\text{eff}}} \text{Log} \left(\frac{4\mu_{e\chi} T_{\text{eff}}}{2m_V^2} \right)$ relative the post-recombination rate, Γ_χ.

We can estimate the typical size of this factor at recombination by taking $T_{\text{eff}} = 0.25$ eV which is the temperature of the plasma at recombination. In that case Δ/T_{eff} is $\sim \mathcal{O}(10^{-5})$. The log enhancement factor is $\mathcal{O}(10 - 20)$ depending on the mediator mass, thus the overall suppression of the DM-electron energy transfer rate prior to recombination is $\mathcal{O}(10^{-3})$ relative to the DM-hydrogen rate post-recombination. This implies that the energy transfer rate is slightly lower in the pre-recombination era.

In the region of parameter space which we dubbed as our strong coupling regime, this would not significantly alter the initial conditions since the DM would be tightly coupled to the plasma both before and after recombination. Thus, it is expected, that in the strong coupling scenario, the DM has a temperature equal to the plasma temperature at recombination as we have assumed, even if other interactions are present in the dark sector. We will discuss constraints on such tight coupling of DM to the plasma at recombination in section 7.

In the weak coupling scenario, the DM is kinetically decoupled post-recombination. Since the coupling is weak, we would also expect the DM to be decoupled prior to recombination. Thus, we would expect that the DM in the pre-recombination era was adiabatically cooling relative to the plasma, and we might expect it to be colder than the plasma temperature at recombination. However, if other interactions of the DM other than those considered in our model are important, it is possible that they could keep the DM at (or near) the same temperature as the plasma even in this scenario, thus providing a justification for our initial conditions.

Alternatively, one could ask what would happen in the weak coupling scenario if the dark matter is colder than the plasma temperature at recombination. If the dark matter is colder than the gas temperature by a factor of $\epsilon < 1$, then in this scenario, the DM would begin adiabatically cooling from this initial value and thus T_χ (or equivalently T_{eff}) would be a factor of ϵ colder at $z = 17$ as well, compared to our expectation of eq. 5.10. This would lower the value of x_D needed at $z = 17$ to attain the pinned value of δT_b by a factor of ϵ. Since, $x_D \propto \alpha_\chi \alpha_e T_{\text{eff}}^{1/2}$, this would lower the value of $\alpha_\chi \alpha_e$ by a factor of $\sqrt{\epsilon}$ compared to the expectation of eq. 5.12. Thus, the allowed couplings of the weak coupling scenario in our parameter space of interest in fig. 1 would be lowered by a factor of $\sqrt{\epsilon}$ for every value of the

DM mass in the weak coupling regime[7].

6.2 Allowed range of mediator masses

The Born approximation that we have used in our cross-section calculations when determining electron DM scattering amplitudes is valid when $\alpha_\chi \alpha_e \mu^2 \ll m_V^2$ (see for e.g. ref. [61]), where μ is the reduced mass of DM and hydrogen (which is approximately the same as the DM mass for most of our benchmark parameter space).

On the other hand, we have also assumed an upper bound on the mediator mass in eq. A.35 in appendix A.2, in order to ensure that the forward scattering divergence of the spin-flip cross-section is dominantly cut-off by the inelastic splitting Δ between the hyperfine states.

These two conditions together imply a mass range for the mediator which is,

$$0.1 \text{ eV} \sqrt{\frac{\alpha_\chi \alpha_e}{10^{-18}}} \left(\frac{\mu}{0.1 \text{ GeV}} \right) \lesssim m_V \lesssim 2.3 \text{ eV} \sqrt{\left(\frac{1000 \text{ K}}{T_{\text{eff}}} \right) \left(\frac{\mu}{0.1 \text{ GeV}} \right)}. \tag{6.3}$$

The allowed range of mediator masses is narrow in the strong coupling scenario that we have considered, but the lower bound relaxes for weaker couplings. In general mediator masses of a few eV are allowed in all scenarios, and mediator masses as low as 10^{-5} eV are allowed by the parameters of our weak coupling scenario, for small enough m_χ.

6.3 Relative velocity between baryons and dark matter

The dark matter and baryons in standard cosmology are expected to have a relative velocity due to the baryons being dragged with the photons before decoupling and then falling back into DM potential wells [62, 63]. This velocity is usually assumed to be Gaussian distributed, with a standard deviation of 29 km/s at $z = 1010$. The dissipation of this relative velocity could lead to a heating of both the baryons and dark matter in the post-recombination era [64].

In our model, the pre-recombination physics that sets the initial conditions would determine the relative velocity (if any) between the DM and baryons. If the DM is tightly kinetically coupled to the baryons till recombination (as is expected to happen in the strong and intermediate coupling scenarios), then the DM would also be dragged with the baryons and we would not expect a relative velocity between the DM and the gas[8]. If the DM is not kinetically coupled to the baryons pre-recombination (as could happen in the weak coupling scenario), then it is possible to have a relative velocity between the DM and the gas. However, as long as the DM is sufficiently cold, this would still lead to a low T_{eff} and hence also a strong broadband absorption signal.

We have not taken into account the relative velocity between DM and baryons in our calculations of the temperature evolution equations.

---

[7]This argument works for moderate ϵ say $1/5, 1/10$ or $1/100$. However, for much smaller values of ϵ, the rates Γ_H and Γ_χ are enhanced at the initial conditions by the small effective temperature (see Eqs. 4.5, 4.6) and we expect that this would lead to rapid energy exchange between the DM and gas till the DM temperature is heated up, such that ϵ is back in the moderate regime.

[8]Such a scenario is ruled out for $f \gtrsim 0.01$ by CMB observations as we will discuss in the next section.

7 Constraints on our model

In this section we will discuss several different categories of constraints on our model. We will attempt to synthesize these constraints and compare with the parameter space of interest in fig. 1.

1. **Laboratory experiments:** The axial-vector boson V generates an effective long-range spin-dependent interaction potential between electrons (and/or positrons). This potential has the form $V(r) = \frac{\alpha_e}{r} \left(\vec{S}_1 \cdot \vec{S}_2 \right) e^{-r/\lambda}$, where $\lambda = \frac{\hbar c}{m_V}$ gives the range of the interaction and $\vec{S}_{1,2}$ denotes the spin of the interacting particles.

   For the mass range of interest (m_V between 10^{-4} eV and 10 eV, see sec. 6.2), the force operates over a range between 10 nm to a few mm, with the shortest range of interactions being of most relevance for our strongly interacting scenario, whereas the full range is of interest for our weakly interacting scenario. Various probes of such spin-dependent forces between electrons have constrained the allowed values of α_e for different interaction ranges/mediator masses. A summary plot of the exclusion curves in the range of interest is shown in Fig. 8.

   For masses $m_V \gtrsim 10$ eV, the strongest constraint is $\alpha_e \lesssim 6 \times 10^{-12}$ which is set by a precision measurement of the hyperfine splitting interval of the positronium ground state [65]. For the range $0.5 \lesssim m_V \lesssim 50$ eV, the most stringent constraint on α_e has been imposed by using Double Electron Electron Resonance (DEER) measurements of the coupling between two electron spins located at two ends of a molecular ruler [66]. The constraint set by these measurement is $\alpha_e \lesssim 4.9 \times 10^{-13}$.
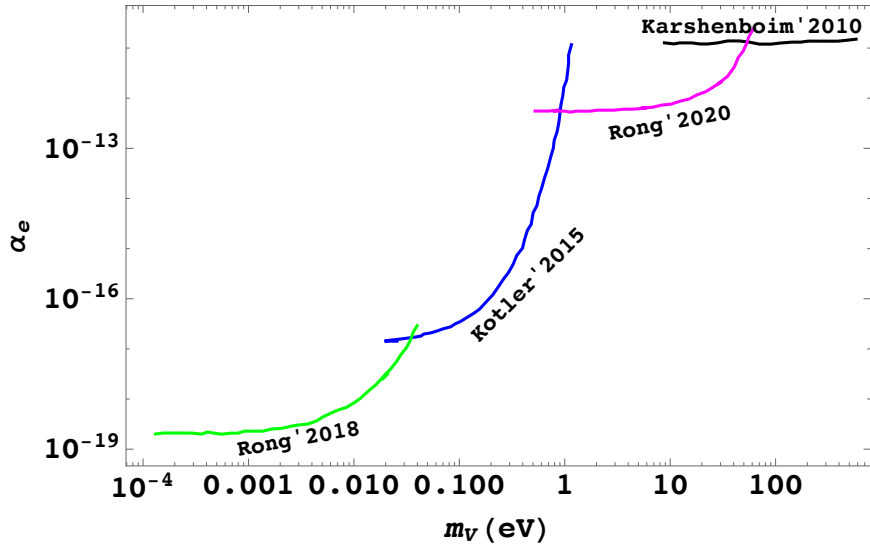

Figure 8: Upper bounds from laboratory experiments on the interaction strength α_e of spin-dependent forces between electrons. The force is assumed to be mediated by an axial-vector boson with a mass m_V in the range 10^{-4} eV - 100 eV. The black, magenta, blue and green lines represent bounds on α_e obtained in refs. [65–68], respectively.

For 0.001 eV $\leq m_V \leq 0.1$ eV, the strongest constraints on exotic spin-dependent dipole-dipole interactions has been obtained by measuring the magnetic interaction between two trapped ^{88}Sr$^+$ ions [67], and this sets a bound $\alpha_e \lesssim 1.2 \times 10^{-17}$. For a mass range $10^{-4} \lesssim m_V \lesssim 10^{-2}$ eV, the strongest constraint comes from single nitrogen valency centers in diamond which can be used as quantum sensors for detecting weak magnetic signals [68]. The constraint in this range of mediator masses is $\alpha_e \lesssim 1.8 \times 10^{-19}$.

2. **Collider searches:** The Lagrangian of our effective theory in eq. 2.1 must be UV completed at an effective scale $\Lambda \sim \frac{m_V}{\sqrt{\alpha_e}}/\left(\frac{3g^2}{16\pi^2}\right)$, where g is the Standard Model (SM) $SU(2)_L$ gauge coupling [69]. In general if the axial-vector boson is coupled to a non-conserved SM fermion current, then in the simplest UV completions, additional fermions must be introduced below the cut-off scale to make the theory anomaly free. Integrating these fermions out of the effective theory generates anomalous interactions between the vector V and the SM gauge bosons [70, 71]. These anomalous interactions would lead to phenomenological signatures such as the exotic Z boson decay $Z \to \gamma V$, which are enhanced by a factor of $(m_Z/m_V)^2$ due to the Goldstone equivalence relation, which dictates that the coupling of the Z to V is dominantly to the longitudinal mode of V.

   The anomalous decay branching fraction then has the form,

   $$\mathrm{Br}(Z \to \gamma V) \simeq 10^{-7} \mathcal{A}^2 \left(\frac{\mathrm{TeV}}{m_V/\sqrt{4\pi\alpha_e}}\right)^2, \tag{7.1}$$

   where $\mathcal{A}$ is in general an $\mathcal{O}(1)$ anomaly coefficient. If V then decays invisibly or is long-lived and escapes the detector, then LEP searches for single photons at half the Z energy limit this branching ratio to be $\lesssim 10^{-6}$ [72, 73]. Applying this bound, we get the stringent limit,

   $$\alpha_e \lesssim 10^{-24} \left(\frac{m_V}{1\ \mathrm{eV}}\right)^2. \tag{7.2}$$

   However, in deriving this limit we needed to assume that the cut-off Λ (or the heavy fermion masses) are larger than the Z mass, which is not true for the parameter space of interest. Thus, if additional fermions are introduced below the Z mass scale, the most stringent constraints would likely arise from Z decays to these exotic fermions, but the details of such a constraint would be model dependent.

   While the constraint derived from anomalous Z decays is strong and rules out the parameter space that we have focused on, it is also contingent on the UV completion. It is possible that more exotic UV completions of our model which violate the electroweak symmetry of the Standard Model may evade these constraints [70].

3. **Constraints from stellar cooling**: The weakly interacting light mediator V could be produced inside the hot and dense interior of stars and would consequently lead to anomalous cooling, which is strongly constrained. The constraints on axial-vector couplings can be inferred through constraints imposed on an equivalent axion (a) couplings, since the dominant production mode of the axial-vector is via the longitudinal mode which behaves like a pseudo-scalar axion [71]. The equivalence can be captured through a change of the effective interaction term in the Lagrangian,

$$\mathcal{L} \supset g_e \bar{e} \gamma^5 \gamma^\mu e V_\mu \sim \frac{1}{2f_a} \bar{e} \gamma^5 \gamma^\mu e \, \partial_\mu a \to -i g_{ae} \bar{e} \gamma^5 e \, a, \tag{7.3}$$

where the first relationship follows from the Goldstone equivalence principle and the identification of $g_e V_\mu \to \frac{1}{f_a} \partial_\mu a$, where the equivalent axion-decay constant $f_a = \frac{m_V}{g_e}$. The second relation follows from an integration by parts and application of the equations of motion, followed by the identification $g_{ae} = \frac{m_e}{f_a}$, where m_e is the mass of electron.

Limits from a combined analysis of the tip of the red-giant branch in the globular cluster M5, anomalous white dwarf cooling, and horizontal branch stars/red giants in globular clusters gives the most stringent constraint on $g_{ae} < 2.6 \times 10^{-13}$ at 95% CL [74, 75].We can convert this to a constraint on α_e as,

$$\alpha_e \lesssim 10^{-38} \left(\frac{m_V}{1 \text{ eV}} \right)^2. \tag{7.4}$$

Once again this is a strong bound which rules out our parameter space of interest, but the constraint is model dependent. For example, the mediator particles can remain trapped inside stars if they have strong self-interactions [76, 77], considerably weakening the constraints. Alternatively, with a chameleon-like mechanism, the mediator could acquire a heavy effective mass inside dense media which prevents it from being produced in the first place [78–80].

4. **Constraints on extra radiation species:** The light axial-vector bosons can potentially contribute to the effective number of relativistic degrees of freedom in the early universe. The number of extra radiation species is usually parameterized in terms of extra neutrino species as ΔN_{eff}. There exist strong constraints on $\Delta N_{\text{eff}} \lesssim 0.1$ from both BBN [81] and CMB [58] data.

   These constraints can be evaded if a) the axial-vector V is not in thermal equilibrium with the SM plasma and is colder than the neutrino temperature b) V is short-lived and decays before BBN, and thus does not form a thermal bath. The first possibility is ruled out since, for our parameter space of interest, V would be strongly kinetically coupled to the plasma. The second possibility could occur either through the loop-process $V \to \gamma\gamma\gamma$ or a neutrino decay process $V \to \nu\bar{\nu}$. The latter reaction might occur in generic gauge-invariant UV completions of our model.

   Another possibility is that the extra radiation species could potentially ameliorate the Hubble H_0 and σ_8 tensions if it is self-interacting [82].

5. **Constraints from kinetic decoupling:** The pre-recombination physics determines whether the DM particle χ is kinetically coupled to the gas at recombination. A fraction of the DM greater than $f \sim 0.01$ which is tightly coupled to the plasma at recombination is ruled out by observations of the CMB [83–85]. Thus, the strong and intermediate coupling scenarios for $f = 1, 0.1$ are ruled out. However, for the smaller benchmark fractions $f = 0.01, 0.001$, in the strong coupling scenario, the additional tightly coupled DM is indistinguishable from a small additional baryon content in terms of its effect on the CMB.

6. **Constraints on self-interaction coupling of DM:**

The light axial-vector mediator can also mediate self-interaction between DM particles. In our case, the self-scattering DM cross-section has the form (appendix. B),

$$\sigma(\chi\chi \to \chi\chi) = 24\pi \frac{\alpha_\chi^2}{m_\chi^2 v^4} \log\left(\frac{m_\chi^2 v^2}{m_V^2}\right), \tag{7.5}$$

with v being the relative velocity for scattering. Observations of the Bullet-cluster and other halo shape observations set strong bounds on DM self-interactions (see ref. [86] for a review),

$$\frac{\sigma}{m_\chi} \lesssim (1 - 10) \text{ cm}^2/\text{g}. \tag{7.6}$$

For $v = 1000$ km/s in a typical galaxy cluster, the coupling is constrained to be,

$$\alpha_\chi \lesssim 10^{-6} \times \left(\frac{m_\chi}{0.1 \text{ GeV}}\right)^{3/2}. \tag{7.7}$$

However, this constraint would only apply if the self-interacting DM is an $\mathcal{O}(1)$ fraction of the whole DM of the universe.

7. **Dark Matter relic abundance and freeze-out:** We have assumed that our DM is asymmetric, but if we had assumed it were produced symmetrically, we would have strong constraints on the coupling α_χ from the condition that the annihilation process $\chi\chi \to VV$ does not deplete the relic abundance, i.e. the cross-section for this process should be smaller than the freeze-out cross-section needed to yield a relic density with a fraction f of the present day DM density, $\sigma v \lesssim \frac{3\times10^{-26}}{f} \text{cm}^3 \text{ s}^{-1}$. This would lead to a bound $\alpha_\chi \lesssim 10^{-5} \times \left(\frac{m_\chi}{0.1 \text{ GeV}}\right) \times \frac{1}{\sqrt{f}}$.

7.1 Summary of constraints:

To summarize, there are two main, robust constraints – a) the constraint from kinetic decoupling and b) the constraint from laboratory experiments on light mediators. Constraints from colliders, stellar cooling, and ΔN_{eff} can be relaxed completely in extensions of our effective theory. The self-interaction constraint only applies for $f = 1$. Also, the freeze-out constraint does not apply, since we assume that χ is produced asymmetrically.

The kinetic decoupling constraint rules out the benchmark parameter space for the strong and intermediate coupling scenarios for $f = 0.1, 1$. For $f = 1$, in the weak coupling regime, $m_\chi \sim 10^{-2}$ GeV, and therefore the upper end of the allowed mediator mass is $m_V \sim 1$ eV (see eq. 6.3). For this mediator mass, laboratory constraints set a limit $\alpha_e \lesssim 10^{-13}$ (see fig. 8). Also, self-interacting DM constraints yield $\alpha_\chi \lesssim 10^{-7}$. Thus, the combination of these two constraints also rules out the benchmark parameter space of the weak coupling scenario for $f = 1$. However, since the self-interaction bound does not apply for $f = 0.1$, the weak coupling parameter space is viable for $f = 0.1$ with moderate values of $\alpha_\chi \sim 0.1$.

For all scenarios with $f = 0.01, 0.001$ and for a mediator mass near the upper end of our allowed range, with moderate values of $\alpha_\chi \sim 0.1$, we would find the entire region of couplings in our benchmark signal parameter space of fig. 1 to be consistent with the laboratory constraints on light mediators in fig. 8.

8   Summary, conclusions, and future directions

Standard cosmology predicts two relatively weak and distinct, band-limited absorption features in the global 21 cm signal near 20 MHz and 90 MHz due to collisional gas dynamics and Ly-α photons from the first stars, respectively. Excess gas cooling models invoked to explain the anomalous EDGES absorption signal also predict the same distinct band-limited absorption features, although these features are predicted to be deeper than those of the standard cosmology.

In the current work, we have explored an alternative prediction of the global 21 cm signal in a model where dark matter interacts with electrons through a light axial vector mediator. This interaction leads to two distinct cosmological effects, the first is a predicted coupling x_D of the gas spin temperature to a new effective temperature scale $T_{\text{eff}} = \mu \left(\frac{T_\chi}{m_\chi} + \frac{T_K}{m_H} \right)$, and the second is a coupling of the gas kinetic temperature to the DM temperature. Through an explicit Born level calculation of these interaction rates, we have found that the spin-flip rate is larger than the kinetic energy transfer rate, which leads to characteristic predictions of our model which distinguish it from the excess gas cooling models.

We have found, generically, that our model leads to predictions of a single, strong, broadband absorption feature which is unlike that of either the standard cosmology or excess gas cooling models. The signal is strong because of the low temperature scale T_{eff} and it is broadband because of the dominance of the spin-flip coupling x_D over the other couplings (collisional, CMB) of the spin temperature for much of the post-recombination cosmological history.

As a benchmark, we have focussed on regions of parameter space in our model which lead to an absorption signal with strength $\delta T_b \simeq -500$ mK at $z = 17$, consistent with the magnitude of the EDGES absorption signal at this redshift. However, this was only used as a benchmark to pin our absorption signal, and we have made no demands on the shape of the spectrum.

In different regions of our model parameter space, we have found, through numerical studies backed by analytic estimates, different predictions for the predicted global 21 cm signal, depending upon the cosmological relevance of the kinetic energy transfer rate. We classified our parameter space of interest into three scenarios of strong, intermediate and weak coupling. While all scenarios predict a single, strong broadband absorption signal, they differ in the detailed predictions.

In the strong coupling scenario, the kinetic energy transfer rate is important over most of the cosmological history, from recombination to the cosmic dawn, and it ensures a tight coupling between the DM and the gas. The spin temperature is also tightly coupled to the adiabatically cooling DM-gas temperature during this same period. This scenario thus leads to a prediction of a strong absorption signal that begins at 5 MHz and extends up to 89 MHz, where it is expected to rise due to a combination of X-ray heating and Ly-α coupling.

In the intermediate coupling scenario, the kinetic energy transfer rate starts off as cosmologically relevant near recombination, but becomes less relevant at lower redshifts. Once again this scenario leads to a strong broadband signal, but in this scenario, the absorption signal begins at lower frequencies than 5 MHz, with a minima at frequencies lower than 89 MHz.

In the weak coupling scenario, the kinetic energy transfer rate is completely irrelevant over the cosmological history. In this scenario, the spin-temperature couples to the adiabatically cooling DM temperature and thus leads to very strong absorption signals at high

redshifts ($z \sim 1000$ or $\nu = 1.4$ Mhz). As the coupling x_D becomes weaker than the coupling to the CMB temperature, δT_b rises, leading to a minimum in the absorption signal deep in the cosmic dark ages.

Above 89 MHz, in both the intermediate and weak coupling scenarios, depending upon the history of X-ray heating of the gas and Ly-α coupling induced by the first stars, δT_b is expected to either rise rapidly, or a second absorption dip might possibly be seen before the rise.

Our calculation of the DM induced hyperfine transition rate showed that the relevant cross-section scales as $1/\Delta^2$, where Δ is the hyperfine splitting. This allows for a large transition rate even for relatively small couplings between the DM and electrons. We explored several constraints on these couplings from terrestrial experiments and astrophysical and cosmological probes. While collider and stellar cooling constraints are strong and would naively rule out the regions of parameter space that we have explored, these constraints may possibly be evaded under extensions of our effective field theory. The more robust constraints demand that the DM particle responsible for spin-flip interactions is asymmetric, and makes up a fraction $f \lesssim 0.1$ of the total DM relic density. We also found that only the weak coupling scenario is viable for $f = 0.1$, based upon CMB constraints of kinetic coupling of the DM to the plasma at recombination. However, for smaller values of $f = 0.01, 0.001$, we found that the strong/weak/intermediate couplings are all viable.

Besides the global 21 cm absorption signal, there are several secondary signatures that can be tested in both cosmic and laboratory settings. We list these secondary tests below:

Astrophysical and cosmological probes:

- While we have not made detailed predictions of the stochastic 21 cm signal, it would be interesting to see the differences between the power spectrum of 21 cm fluctuations predicted in our model and standard cosmological models. The anisotropy signal could be tested by future experiments such as SKA or even more futuristic space based anisotropy measurements.

- We have seen in the weak and intermediate coupling scenarios that the gas spin temperature and kinetic temperature may have different evolutions. While the 21 cm absorption signal would probe the spin temperature, if we had an independent probe of the gas kinetic temperature we could measure the deviation between T_s and T_K, this would be an additional test of the spin-flip mechanism that we have proposed. The challenge would be to find a probe that is independently sensitive to the gas kinetic temperature at a redshift before reionization. One example of such a probe could be a measurement of the pressure-smoothing scale [87] which is sensitive to the integrated thermal history of the intergalactic medium (IGM) [88]. However, this probe is mostly sensitive to the low redshift thermal history of the IGM post-reionization.

Particle physics probes:

- Since the axial-vector V couples to an anomalous current, generically UV extensions of our model that are anomaly free would lead to decay $Z \to \gamma V$. In order to evade the strong constraints on such anomalous Z decays, one would need to build a UV model with broken SM gauge symmetries. Such models could lead to interesting testable predictions at collider experiments.

- In the strong coupling regime, the mediator mass is tightly constrained to be around 1 eV in order to evade constraints from laboratory searches for spin-dependent interactions between electrons. However, increasing the sensitivity of these laboratory searches by an order of magnitude could rule out the strong/intermediate coupling scenarios proposed in our work, or potentially discover the mediator particle.

The strong broadband signal that we have proposed in this work has exciting implications for global 21 cm signal experiments. Searching for this signal would require experiments to change their search strategies in order to discover the signal as compared to the typical band-limited search strategies motivated by standard cosmology. Specific examples of such changes would be use of alternative templates to extract the cosmological signal from the foreground dominated map, and comparing the extracted signal across experiments probing different regions of the radio spectrum. We have also suggested several secondary tests that could validate the particle physics origin of such a cosmological signal. We leave a more detailed exploration of these tests to future work.

Acknowledgments

A Rate for excitation of hydrogen from the singlet to triplet state via dark matter scattering

In this appendix we will work out the rate for excitation and de-excitation of neutral hydrogen from the ground state (H_0) to the excited state (H_1), i.e. for the process

$$\chi + H_0 \rightleftarrows \chi + H_1. \tag{A.1}$$

In appendix A.1, we will work out the amplitude for excitation and de-excitation including the details of the bound state wave function of the electron. In appendix A.2, we use these amplitudes to compute the reaction rates for the forward and backward spin-flip reactions D_{01} and D_{10}. In appendix A.3, we use these amplitudes to compute the energy transfer rate or equivalently the temperature equilibration time scale between the dark matter and gas.

A.1 Amplitude for excitation and de-excitation

Let us first consider the excitation process with specific spin states,

$$\chi_s + H_0 \rightarrow \chi_{s'} + H_{1,s'_H}, \tag{A.2}$$

where s and s' denote the spin state of the dark matter particle χ, and s'_H denotes the spin state of the final state triplet.

A.1.1 Bound state wave functions

We first express the bound state wave function of a hydrogen atom in either the singlet or triplet states moving with velocity $\vec{v}$ in terms of free proton and electron states as,

$$|H_0(\vec{v})\rangle = \sqrt{\frac{2m_H}{2m_e 2m_p}} \int \frac{d^3k}{(2\pi)^3} \tilde{\psi}_{1s}(\vec{k}) \frac{1}{\sqrt{2}} [|p(-\vec{k} + m_p\vec{v}, \downarrow)\rangle \otimes |e(\vec{k} + m_e\vec{v}, \uparrow)\rangle$$
$$- |p(-\vec{k} + m_p\vec{v}, \uparrow)\rangle \otimes |e(\vec{k} + m_e\vec{v}, \downarrow)\rangle], \qquad (A.3)$$

for the singlet state, and

$$|H_1(\vec{v})\rangle = \sqrt{\frac{2m_H}{2m_e 2m_p}} \int \frac{d^3k}{(2\pi)^3} \tilde{\psi}_{1s}(\vec{k}) \frac{1}{\sqrt{2}} [|p(-\vec{k} + m_p\vec{v}, \downarrow)\rangle \otimes |e(\vec{k} + m_e\vec{v}, \uparrow)\rangle$$
$$+ |p(-\vec{k} + m_p\vec{v}, \uparrow)\rangle \otimes |e(\vec{k} + m_e\vec{v}, \downarrow)\rangle], \qquad (A.4)$$

for the triplet state which has spin $s'_H = 0$ along a chosen spin quantization z-axis. Note that the choice of spin quantization axis here is arbitrary. One can similarly write down the $s'_H = \pm 1$ states for the triplet by suitable choice of the proton and electron spins ($\uparrow\uparrow$ for the $s'_H = 1$ state and $\downarrow\downarrow$ for the $s'_H = -1$ state). In these expressions, m_H, m_e and m_p denote the masses of hydrogen, the electron, and proton, respectively. $\vec{k}$ denotes the relative internal momentum between the proton and electron. We have neglected the mass difference of the singlet and triplet states in the normalization of the wave-functions. The Fourier transform of the hydrogen $1s$ state wave-function is given by,

$$\tilde{\psi}_{1s}(\vec{k}) = \frac{8\sqrt{\pi}}{a_0^{5/2}} \frac{1}{\left(k^2 + \frac{1}{a_0^2}\right)^2}, \qquad (A.5)$$

where a_0 is the Bohr radius. The free particle p and e states have the standard relativistic normalization. For example, for the proton state we have,

$$\langle p(q_1, s_1)|p(q_0, s_0)\rangle = 2m_p \delta_{s_1 s_0} (2\pi)^3 \delta^3(\vec{q_1} - \vec{q_0}), \qquad (A.6)$$

where $\vec{q}$ is the momentum of the proton state and s_0 (s_1) denotes the z component of spin of the initial (final) state.

A.1.2 Amplitude for excitation

We take the reaction,

$$\chi_s + H_0 \rightarrow \chi_{s'} + H_1. \qquad (A.7)$$

and assign a velocity $\vec{v}_0$ and $\vec{v}_1$ to the singlet and triplet hydrogen atoms, respectively.

In order to evaluate the amplitude for this process, we first need to find the amplitude for the free particle process

$$\chi_s + e^-_{s_e} \rightarrow \chi_{s'} + e^-_{s'_e}, \qquad (A.8)$$

which occurs through the t-channel exchange of the light mediator, and then insert it between the bound state wave functions discussed previously. Here, s_e and s'_e denote the spin state

of the initial and final state electrons. Using the Lagrangian in eq. 2.1, this amplitude can be evaluated at tree-level as

$$\mathcal{M} = \frac{g_\chi g_e}{(q^2 - m_V^2)} \bar{u}(p_{\chi'}, s') \gamma^\mu \gamma^5 u(p_\chi, s) \bar{u}(p'_e, s'_e) \gamma_\mu \gamma^5 u(p_e, s_e) \tag{A.9}$$

We have assigned 4-momenta p_χ (p'_χ) and p_e (p'_e) to the dark matter and electron, respectively for the initial state (final state). We have also defined the momentum transfer q as,

$$q^2 \equiv (p'_\chi - p_\chi)^2 = (p_e - p'_e)^2. \tag{A.10}$$

In the non-relativistic limit we can show that the amplitude eq. A.9 can be written as [89],

$$\mathcal{M} \simeq -16 \frac{g_\chi g_e}{(q^2 - m_V^2)} m_\chi m_e \langle s', s'_e | \vec{S}_\chi \cdot \vec{S}_e | s, s_e \rangle, \tag{A.11}$$

where $\vec{S} = \frac{1}{2}\vec{\sigma}$ denotes the spin projection operator and $\vec{\sigma}$ are Pauli matrices. We can further write

$$\vec{S}_\chi . \vec{S}_e = \frac{1}{4} \left(2(\sigma_\chi^+ \sigma_e^- + \sigma_\chi^- \sigma_e^+) + \sigma_\chi^z \sigma_e^z \right), \tag{A.12}$$

where σ^z is the diagonal Pauli matrix, and we have used the spin raising and lowering operators written in terms of the Pauli matrices $\sigma^\pm = \frac{1}{2}(\sigma^x \pm i\sigma^y)$. Thus, the matrix element in the scattering amplitude can be evaluated as,

$$\langle s', s'_e | \vec{S}_\chi \cdot \vec{S}_e | s, s_e \rangle = \begin{matrix} & \uparrow\uparrow & \uparrow\downarrow & \downarrow\uparrow & \downarrow\downarrow \\ \begin{pmatrix} \frac{1}{4} & 0 & 0 & 0 \\ 0 & -\frac{1}{4} & \frac{1}{2} & 0 \\ 0 & \frac{1}{2} & -\frac{1}{4} & 0 \\ 0 & 0 & 0 & \frac{1}{4} \end{pmatrix} & \begin{matrix} \uparrow\uparrow \\ \uparrow\downarrow \\ \downarrow\uparrow \\ \downarrow\downarrow \end{matrix} \end{matrix}, \tag{A.13}$$

where the column (row) labels refer to the spin of the outgoing (incoming) dark matter and electron respectively. Using the $e\chi \to e\chi$ scattering amplitude, we can now evaluate the hydrogen excitation amplitude by using the bound state wave functions. In the non-relativistic limit we can identify the 4-vector momentum transfer as $q \simeq (0, m_H(\vec{v}_0 - \vec{v}_1)) \equiv (0, \vec{q})$.

We can then write the resulting amplitudes for all spin combinations in terms of the following master amplitude which we denote as $\mathcal{M}_0$,

$$\mathcal{M}_0 = 4\sqrt{2} g_\chi g_e \frac{m_H m_\chi}{q^2 - m_V^2} F(q^2) \tag{A.14}$$

where $F(q^2)$ is the hydrogen atom form factor,

$$F(q^2) = \int \frac{d^3 k}{(2\pi)^3} \tilde{\psi}_{1s}(\vec{k}) \tilde{\psi}_{1s}^*(\vec{k} + \vec{q}), \tag{A.15}$$

$$= \left(\frac{1}{1 + \frac{q^2 a_0^2}{4}} \right)^2, \tag{A.16}$$

$$\to 1 \text{ for } q^2 \ll \frac{1}{a_0^2}. \tag{A.17}$$

The full amplitudes are non-zero only for the following spin combinations,

$$\mathcal{M}(\chi(s =\uparrow) + H_0 \to \chi(s' =\downarrow) + H_1(s'_H = 1)) = \mathcal{M}_0, \tag{A.18}$$

$$\mathcal{M}(\chi(s =\downarrow) + H_0 \to \chi(s' =\uparrow) + H_1(s'_H = -1)) = -\mathcal{M}_0, \tag{A.19}$$

$$\mathcal{M}(\chi(s =\uparrow) + H_0 \to \chi(s' =\uparrow) + H_1(s'_H = 0)) = -\frac{1}{\sqrt{2}}\mathcal{M}_0, \tag{A.20}$$

$$\mathcal{M}(\chi(s =\downarrow) + H_0 \to \chi(s' =\downarrow) + H_1(s'_H = 0)) = \frac{1}{\sqrt{2}}\mathcal{M}_0, \tag{A.21}$$

where s'_H denotes the z component of the spin of the final state triplet. Squaring the amplitude and taking a spin-sum over final states and averaging over initial states we get,

$$\frac{1}{(2S_\chi + 1)(2S_0 + 1)} \sum_{\{\text{spins}\}} |\mathcal{M}|^2 = \frac{3}{2}|\mathcal{M}_0|^2, \tag{A.22}$$

where $S_\chi = 1/2$, $S_0 = 0$ are the spins of χ and H_0 respectively.

A.1.3   Amplitude for de-excitation

For the de-excitation process, we can similarly show that the spin-summed and averaged amplitude is given by

$$\frac{1}{(2S_\chi + 1)(2S_1 + 1)} \sum_{\{\text{spins}\}} |\mathcal{M}|^2 = \frac{1}{2}|\mathcal{M}_0|^2, \tag{A.23}$$

where $S_1 = 1$ is the spin of the triplet H_1.

A.2   Excitation and de-excitation rates

We will now use the amplitudes that we have computed to work out the excitation and de-excitation rates. The rate for excitations $\chi + H_0 \to \chi + H_1$ is given by,

$$D_{01} \equiv n_\chi \langle \sigma_{01} v_{\text{rel}} \rangle$$

$$= n_\chi (2\pi)^6 \int \frac{d^3 p_i}{(2\pi)^3 2E_i} \frac{d^3 p_0}{(2\pi)^3 2E_0} \frac{d^3 p_f}{(2\pi)^3 2E_f} \frac{d^3 p_1}{(2\pi)^3 2E_1} f(p_i) f(p_0)$$

$$\times \frac{1}{(2S_\chi + 1)(2S_0 + 1)} \sum_{\{\text{spins}\}} |\mathcal{M}|^2 (2\pi)^4 \delta^{(4)}(p_i + p_0 - p_f - p_1), \tag{A.24}$$

where we have taken p_i and p_0 to be the momenta of the initial dark matter particle and singlet H_0, respectively and p_f and p_1 to be the momenta of the final state dark matter particle and triplet H_1. The distribution functions for the initial particles are taken to be of the form $f(p_i) = \frac{1}{(2\pi m_\chi T_\chi)^{3/2}} e^{-\frac{p_i^2}{2m_\chi T_\chi}}$ and $f(p_0) = \frac{1}{(2\pi m_H T_K)^{3/2}} e^{-\frac{p_0^2}{2m_H T_K}}$, where T_χ is the temperature of the dark matter and T_K the gas temperature. We can now change integration variables for the initial state particles by defining the relative momenta $\vec{p}$ and a conjugate momentum variable $\vec{p}_m$,

$$\vec{p} \equiv \mu \vec{v}_{\text{rel}} = \mu \left(\frac{\vec{p}_0}{m_H} - \frac{\vec{p}_i}{m_\chi} \right), \tag{A.25}$$

$$\vec{p}_m = M \left(\frac{\frac{\vec{p}_0}{T_K} + \frac{\vec{p}_i}{T_\chi}}{\frac{m_H}{T_K} + \frac{m_\chi}{T_\chi}} \right), \tag{A.26}$$

where $\vec{v}_{\rm rel}$ is the relative velocity between the initial state particles, $\mu = m_H m_\chi/(m_H + m_\chi)$ is the reduced mass of dark matter and hydrogen and $M = m_H + m_\chi$ is their mass sum. Then we can replace,

$$\int d^3 p_i d^3 p_0 f(p_i) f(p_0) \to \int d^3 p d^3 p_m f(p) f(p_m) \tag{A.27}$$

where the effective distribution functions for p and p_m are given respectively by,

$$f(p) = \frac{1}{(2\pi \mu T_{\rm eff})^{3/2}} e^{-\frac{p^2}{2\mu T_{\rm eff}}}, \quad \text{and} \tag{A.28}$$

$$f(p_m) = \frac{1}{(2\pi M T_m)^{3/2}} e^{-\frac{p_m^2}{2M T_m}}, \tag{A.29}$$

where we have defined $T_{\rm eff} = \mu \left(\frac{T_\chi}{m_\chi} + \frac{T_K}{m_H} \right)$ and $T_m = \frac{T_K T_\chi}{T_{\rm eff}}$. Making this substitution in eq. A.24 and using the fact that the excitation cross-section only depends on the relative momentum p and not on p_m, we can trivially perform the integration over p_m and write

$$D_{01} = n_\chi \langle \sigma_{01} v_{\rm rel} \rangle = n_\chi \int d^3 p f(p) \sigma_{01} v_{\rm rel}. \tag{A.30}$$

We can evaluate the cross-section in the center-of-momentum frame (COM) and then identify p as the magnitude of incoming momentum of either particle in this frame. In terms of the COM frame scattering angle θ, one can evaluate the cross-section as,

$$\sigma_{01} v_{\rm rel} = \frac{1}{2E_i} \frac{1}{2E_0} \frac{1}{16\pi} \int d(\cos\theta) \frac{2p'}{E_i + E_0} \frac{1}{2} \sum_{\{\rm spins\}} |\mathcal{M}|^2, \tag{A.31}$$

where the final state momentum in the COM frame is $p' \simeq \sqrt{p^2 - p_{\rm th}^2}$ and $p_{\rm th} = \sqrt{2\Delta\mu}$ is the excitation threshold momentum, with Δ being the energy splitting between the singlet and triplet states. The momentum transfer q^2 can be written as $q^2 \simeq -p^2 - p'^2 + 2pp'\cos\theta$. Substituting our expression for the amplitude-squared worked out in the previous sub-section eq. A.22, we obtain

$$\sigma_{01} v_{\rm rel} \simeq \frac{3}{2\pi} g_\chi^2 g_e^2 \mu p' \int_{-1}^{1} d(\cos\theta) \left(\frac{1}{q^2 - m_V^2} \right)^2 F^2(q^2). \tag{A.32}$$

The scattering process is dominated by forward scattering which has a low momentum transfer and thus we can approximate $q^2 \ll 1/a_0^2$, and we can then take the hydrogen form factor $F(q^2) \simeq 1$. The angular integral then simplifies to,

$$\mathcal{I} = \int_{-1}^{1} d(\cos\theta) \left(\frac{1}{-p^2 - p'^2 - m_V^2 + 2pp'\cos\theta} \right)^2, \tag{A.33}$$

$$= \frac{2}{(p_{\rm th}^2 - m_V^2)^2 + 4m_V^2 p^2}, \tag{A.34}$$

where we have also substituted for p' in terms of p and $p_{\rm th}$ in the last line. Note that the angular integration would be singular in the limit that $m_V \to 0$ and $p_{\rm th} \to 0$. This is due to

the usual forward elastic-scattering singularity with a massless mediator. The divergence in the angular integration is cut-off by both the finite mediator mass, as well as by the threshold momentum of the inelastic reaction.

We choose to work in the limit $m_V \to 0$, where the divergence in the angular integral is dominantly cut-off by the threshold momentum for excitations rather than the mediator mass. To be precise, we need to work in the limit $m_V^2 \ll p_{\rm th}^4/p_c^2$, where $p_c^2 = 2\mu T_{\rm eff}$ is the characteristic relative momentum in the thermal distribution[9]. This condition can be expressed as,

$$m_V \ll \sqrt{\frac{2\mu}{T_{\rm eff}}}\Delta \simeq 2.3 \text{ eV} \sqrt{\left(\frac{1000 \text{ K}}{T_{\rm eff}}\right)\left(\frac{\mu}{0.1 \text{ GeV}}\right)}. \tag{A.35}$$

In this limit, we obtain the excitation cross-section as,

$$\sigma_{01} v_{\rm rel} \simeq \frac{3}{4\pi}\frac{g_\chi^2 g_e^2}{\Delta^2}\frac{p'}{\mu}. \tag{A.36}$$

Upon performing thermal averaging, we find

$$\langle\sigma_{01} v_{\rm rel}\rangle \simeq \int d^3p f(p)\sigma_{01} v_{\rm rel}, \tag{A.37}$$

$$= \frac{3}{4\pi}\frac{g_\chi^2 g_e^2}{\Delta^2}\sqrt{\frac{8T_{\rm eff}}{\pi\mu}}e^{-\frac{\Delta}{T_{\rm eff}}}. \tag{A.38}$$

Here, $\langle v_{\rm rel}\rangle = \sqrt{\frac{8T_{\rm eff}}{\pi\mu}}$ is the thermal average relative velocity and the exponential suppression factor is due to thermal suppression of the excitation reaction. Similarly, for the de-excitation cross-section in the limit of negligible mediator mass we obtain,

$$\langle\sigma_{10} v_{\rm rel}\rangle \simeq \frac{1}{4\pi}\frac{g_\chi^2 g_e^2}{\Delta^2}\sqrt{\frac{8T_{\rm eff}}{\pi\mu}}. \tag{A.39}$$

Note the key differences of absence of a factor of 3 (due to fewer final states) and absence of an exponential suppression factor (due to lack of a threshold energy for de-excitation). The excitation and de-excitation rates D_{01} and D_{10} are found by simply multiplying these thermal cross-sections with the number density of dark matter particles at the relevant red-shift. The ratio of rates is given by,

$$\frac{D_{01}}{D_{10}} = 3e^{-\frac{\Delta}{T_{\rm eff}}}. \tag{A.40}$$

The characteristic low momentum DM spin-flip interaction cross-section is given by,

$$\sigma_{01} \simeq 3\sigma_{10} \simeq 12\pi\frac{\alpha_\chi\alpha_e}{\Delta^2} \tag{A.41}$$

$$\simeq 4.2\times10^{-14}\left(\frac{\alpha_\chi}{10^{-2}}\right)\left(\frac{\alpha_e}{10^{-14}}\right) \text{ cm}^2 \simeq 4.2\times10^{10}\left(\frac{\alpha_\chi}{10^{-2}}\right)\left(\frac{\alpha_e}{10^{-14}}\right) \text{ barns,} \tag{A.42}$$

---

[9]This condition is more stringent than the condition $m_V^2 \ll p_{\rm th}^2$ which allows us to neglect the mediator mass in the first term in brackets in the denominator of eq. A.34, but not in the second.

where we have rewritten the coupling constants in terms of $\alpha_\chi = g_\chi^2/4\pi$ and $\alpha_e = g_e^2/4\pi$. The typical relative velocity between the DM and hydrogen is given by $\langle v_{\rm rel} \rangle = \sqrt{8 T_{\rm eff}/\pi \mu} \simeq$ $1.4~{\rm km/s}\sqrt{\left(\frac{T_{\rm eff}}{10~{\rm K}}\right)\left(\frac{0.1~{\rm GeV}}{\mu}\right)}$.

These cross-sections are huge by particle physics standards, and this is all the more surprising given the benchmark couplings we have assume are so weak. The reason for the large cross-section is easy to understand however: ***Since the mass splitting between the singlet and triplet states is tiny, the t-channel scattering of dark matter with these states is almost elastic and therefore has a nearly divergent scattering cross-section driven by the large probability for forward scattering. This divergence is cut-off by the tiny hyperfine mass-splitting between the singlet and triplet states and leads to a large cross-section for the spin-flip interaction.***

The number density of dark matter at a red-shift z can be written as[10]

$$n_\chi = \frac{f \Omega_{\rm DM} \rho_c}{m_\chi}(1+z)^3, \tag{A.43}$$

$$\simeq 1.2 \times 10^{-44} \left(\frac{f}{0.1}\right)\left(\frac{0.1~{\rm GeV}}{m_\chi}\right)\left(\frac{1+z}{1+10}\right)^3~{\rm GeV}^3, \tag{A.44}$$

$$\simeq 1.5 \times 10^{-3} \left(\frac{f}{0.1}\right)\left(\frac{0.1~{\rm GeV}}{m_\chi}\right)\left(\frac{1+z}{1+10}\right)^3~{\rm cm}^{-3}. \tag{A.45}$$

where $\rho_c = 3.63 \times 10^{-47}~{\rm GeV}^4$ is the critical density and $\Omega_{\rm DM} = 0.26$ is the present day DM relic density fraction and we have allowed for the possibility that the species we are considering makes up only a fraction f of the dark matter. Thus, we can write the excitation and de-excitation rates as,

$$D_{10} \simeq \frac{1}{3} D_{01},$$

$$= n_\chi 4\pi \frac{\alpha_\chi \alpha_e}{\Delta^2}\sqrt{\frac{8 T_{\rm eff}}{\pi \mu}}$$

$$= 1.99 \times 10^{-36} \left(\frac{f}{0.1}\right)\left(\frac{0.1~{\rm GeV}}{m_\chi}\right)\left(\frac{\alpha_\chi}{10^{-2}}\right)\left(\frac{\alpha_e}{10^{-14}}\right)\left(\frac{0.1~{\rm GeV}}{\mu}\right)^{\frac{1}{2}}\left(\frac{T_{\rm eff}}{10~{\rm K}}\right)^{\frac{1}{2}}\left(\frac{1+z}{1+10}\right)^3~{\rm GeV},$$

$$= 3.01 \times 10^{-12} \left(\frac{f}{0.1}\right)\left(\frac{0.1~{\rm GeV}}{m_\chi}\right)\left(\frac{\alpha_\chi}{10^{-2}}\right)\left(\frac{\alpha_e}{10^{-14}}\right)\left(\frac{0.1~{\rm GeV}}{\mu}\right)^{\frac{1}{2}}\left(\frac{T_{\rm eff}}{10~{\rm K}}\right)^{\frac{1}{2}}\left(\frac{1+z}{1+10}\right)^3~{\rm s}^{-1}. \tag{A.46}$$

A.3 Kinetic energy transfer rate

The same spin-flip interactions that we had considered $\chi_s + H_0 \leftrightarrows \chi_{s'} + H_{1,s'_H}$, can lead to kinetic energy transfer from the DM to neutral hydrogen and vice-versa. It is also possible to have kinetic energy transfer via the elastic reaction $\chi_s + H_1 \rightarrow \chi_{s'} + H_1$[11], however we will argue that this contribution is sub-dominant.

---

[10]Here, for simplicity we are considering the homogenous dark matter distribution only. At low redshifts there will be a boost to the interaction rate (which can be parameterized as an effective scaling of the number density of dark matter) due to the formation of halos.

[11]This reaction proceeds only through the $s'_H = \pm 1$ states of H_1 without spin-flip. Both the other possible elastic scattering processes, involving the $s'_H = 0$ state of H_1 and the process $\chi + H_0 \rightarrow \chi + H_0$, have vanishing amplitudes.

In this sub-section we will compute the kinetic energy transfer rate and the effect on temperature evolution of the dark matter and neutral hydrogen species.

The temperature evolution of a species can be computed from the second moment of the Boltzmann equation assuming that scattering does not distort the distribution far away from thermal. For the DM species for example, we can write down the temperature evolution equation as,

$$\frac{dT_\chi}{dt} = -2HT_\chi + \frac{2}{3}\dot{Q}_\chi, \tag{A.47}$$

where $\dot{Q}_\chi$ is the dark matter heating rate due to kinetic energy transfer from the hotter hydrogen gas. We can write an expression for $\dot{Q}_\chi$ as,

$$\dot{Q}_\chi \equiv \dot{Q}_\chi^{01} + \dot{Q}_\chi^{10}, \tag{A.48}$$

$$\equiv n_0 R_{01} + n_1 R_{10}, \tag{A.49}$$

where the energy transfer weighted rate coefficient for excitation is R_{01} and for de-excitations is R_{10}. Symbolically, we may express the rate coefficient for excitations as,

$$R_{01} \sim \langle E_T \overline{\sigma}_{01} v_{\text{rel}} \rangle, \tag{A.50}$$

where E_T is the energy transfer and $\overline{\sigma}_{01}$ is the "energy-transfer" cross-section. A more precise definition is as follows,

$$R_{01} = (2\pi)^6 \int \frac{d^3 p_i}{(2\pi)^3 2E_i} \frac{d^3 p_0}{(2\pi)^3 2E_0} \frac{d^3 p_f}{(2\pi)^3 2E_f} \frac{d^3 p_1}{(2\pi)^3 2E_1} f(p_i) f(p_0) \times (E_f - E_i)$$

$$\times \left(\frac{1}{(2S_\chi + 1)(2S_0 + 1)} \sum_{\{\text{spins}\}} |\mathcal{M}|^2 (2\pi)^4 \delta^{(4)}(p_i + p_0 - p_f - p_1) \right). \tag{A.51}$$

A similar expression holds for the de-excitation energy transfer rate coefficient. It is instructive to explicitly show how to evaluate the spin-excitation energy-transfer rate, which we will do for excitations and we will just state the result for de-excitations. We begin by making the change of variables from p_0, $p_i \rightarrow p$, p_m as before. Then, taking the relative momentum to be along the z-axis without loss-of-generality, and defining θ as the scattering angle in the COM frame, the energy transfer can be written as,

$$(E_f - E_i) \simeq \left(\frac{T_K - T_\chi}{T_{\text{eff}}} \right) \left(\frac{p^2}{M} \right) \left(1 - \frac{p'}{p} \cos\theta \right) + \text{linear corrections in } p_m. \tag{A.52}$$

Once again p is the relative momentum in the COM frame of the incoming particles and $p'^2 \simeq p^2 - 2\mu\Delta$ is the outgoing momentum in the COM frame. The linear correction in p_m to the energy transfer is unimportant since it does not contribute once we integrate over all possible directions of p_m. The integration over p_m can once again be performed trivially and we are thus left with an integral over relative momentum p,

$$R_{01} = \int d^3 p f(p) E_T \overline{\sigma}_{01} v_{\text{rel}} \tag{A.53}$$

where $f(p) = \frac{1}{(2\pi\mu T_{\text{eff}})^{3/2}} e^{-\frac{p^2}{2\mu T_{\text{eff}}}}$ and we have schematically written the form of the integrand. The energy transfer weighted rate before thermal averaging is given by,

$$E_T \bar{\sigma}_{01} v_{\text{rel}} \simeq \left(\frac{T_K - T_\chi}{T_{\text{eff}}}\right)\left(\frac{p^2}{M}\right) 3\frac{g_\chi^2 g_e^2}{2\pi}\mu p' \int_{-1}^{1} d\cos\theta \frac{\left(1 - \frac{p'}{p}\cos\theta\right)}{\left(-p^2 - p'^2 - m_V^2 + 2pp'\cos\theta\right)^2} \quad (A.54)$$

$$\simeq \left(\frac{T_K - T_\chi}{T_{\text{eff}}}\right)\left(\frac{p^2}{M}\right) 3\frac{g_\chi^2 g_e^2}{2\pi}\mu p' \left\{\frac{1}{2\mu\Delta p^2} + \text{Log}\left(\frac{4p^4}{\mu^2\Delta^2}\right)\right\} \quad (A.55)$$

$$\rightarrow \left(\frac{T_K - T_\chi}{2}\right)\frac{3}{4\pi}\frac{g_\chi^2 g_e^2}{\Delta^2}\left(\frac{2\Delta\mu}{MT_{\text{eff}}}\right)\frac{p'}{\mu}. \quad (A.56)$$

In the second line above, we see that the forward scattering divergence of the integral is cut-off by the inelastic hyperfine splitting parameter Δ. The divergence has two parts, the leading divergence scales as $1/\Delta$ and a sub-leading piece which scales as $\text{Log}\,\Delta$. In the last line above we have dropped the sub-leading contribution.

Note that in the second line in the equation above we have neglected the mediator mass which could also cut-off the forward divergence. This can be justified if we assume the same upper bound on the mediator mass that we had assumed as in eq. A.35, when calculating the spin-flip rate. However, for the elastic scattering process $\chi + H_1 \rightarrow \chi + H_1$, the forward scattering divergence is cut-off only by the mediator mass. In that case, the corresponding integrand only has a logarithmic divergence, scaling as $\text{Log}\,m_V$, i.e. there is no $1/m_V$ type divergence (see a derivation in Appendix B). Thus, the elastic scattering energy transfer cross-section is suppressed relative to the inelastic cross-section that we have considered here, and hence we will ignore this contribution to the energy transfer.

Now performing the thermal averaging of the rate in eq. A.56 we get,

$$R_{01} \simeq \left(\frac{T_K - T_\chi}{2}\right)\left(\frac{2\Delta\mu}{MT_{\text{eff}}}\right)\frac{3}{4\pi}\frac{g_\chi^2 g_e^2}{\Delta^2}\sqrt{\frac{8T_{\text{eff}}}{\pi\mu}}e^{-\frac{\Delta}{T_{\text{eff}}}}. \quad (A.57)$$

We can similarly evaluate the rate for de-excitation reactions as,

$$R_{10} \simeq \left(\frac{T_K - T_\chi}{2}\right)\left(\frac{2\Delta\mu}{MT_{\text{eff}}}\right)\frac{1}{4\pi}\frac{g_\chi^2 g_e^2}{\Delta^2}\sqrt{\frac{8T_{\text{eff}}}{\pi\mu}}. \quad (A.58)$$

Combining the energy transfer rates from both excitations and de-excitations we get,

$$\dot{Q}_\chi = \Gamma_\chi (T_K - T_\chi), \quad (A.59)$$

where we have defined Γ_χ as the characteristic energy transfer rate. This would correspond to the inverse time-scale to transfer an $\mathcal{O}(1)$ fraction of the baryon kinetic energy to the dark matter.

If we further make the approximation that $n_1 \simeq 3n_0$ (for spin temperature $T_s \gg \Delta$) and using $n_H = n_0 + n_1$, we can write the energy transfer rate Γ_χ as,

$$\Gamma_\chi \simeq n_H \left(\frac{\Delta\mu}{2MT_{\text{eff}}}\right) 12\pi\frac{\alpha_\chi\alpha_e}{\Delta^2}\sqrt{\frac{8T_{\text{eff}}}{\pi\mu}}. \quad (A.60)$$

Upon comparing this with the expression for the rate D_{01} for excitations (eq. A.46) we see that the energy transfer rate is suppressed by a factor of $S \equiv \left(\frac{\Delta\mu}{2MT_{\rm eff}}\right) = 3.42 \times 10^{-4} \left(\frac{10\,{\rm K}}{T_{\rm eff}}\right) \left(\frac{\mu}{0.1\,{\rm GeV}}\right) \left(\frac{1\,{\rm GeV}}{M}\right)$. This is because the energy transfer per collision is not of $\mathcal{O}(T_K - T_\chi)$, but rather since the scattering process is dominantly forwards, the energy transfer is of the order of the mass splitting between the singlet and triplet states, i.e. it is $\mathcal{O}(\Delta)$. Thus, the timescale to transfer an $\mathcal{O}(1)$ fraction of the kinetic energy of the gas to the DM is longer than the interaction time scale by a factor of $\mathcal{O}(T_{\rm eff}/\Delta)$.

Now we can use,

$$n_H = \frac{\Omega_b \rho_c}{m_H}(1+z)^3, \tag{A.61}$$

$$= 2.3 \times 10^{-45} \left(\frac{1+z}{1+10}\right)^3 \, {\rm GeV}^3, \tag{A.62}$$

$$= 3.0 \times 10^{-4} \left(\frac{1+z}{1+10}\right)^3 \, {\rm cm}^{-3}. \tag{A.63}$$

Here, we have used the present-day baryon density fraction $\Omega_b = 0.05$ and we have assumed for simplicity that all the baryons are in the form of neutral hydrogen at the relevant redshifts. Thus, we can write an expression for the rate Γ_χ as,

$$\Gamma_\chi = 3.97 \times 10^{-40} \left(\frac{\alpha_\chi}{10^{-2}}\right) \left(\frac{\alpha_e}{10^{-14}}\right) \left(\frac{1\,{\rm GeV}}{M}\right) \left(\frac{\mu}{0.1\,{\rm GeV}}\right)^{\frac{1}{2}} \left(\frac{10\,{\rm K}}{T_{\rm eff}}\right)^{\frac{1}{2}} \left(\frac{1+z}{1+10}\right)^3 \, {\rm GeV}, \tag{A.64}$$

$$= 6.02 \times 10^{-16} \left(\frac{\alpha_\chi}{10^{-2}}\right) \left(\frac{\alpha_e}{10^{-14}}\right) \left(\frac{1\,{\rm GeV}}{M}\right) \left(\frac{\mu}{0.1\,{\rm GeV}}\right)^{\frac{1}{2}} \left(\frac{10\,{\rm K}}{T_{\rm eff}}\right)^{\frac{1}{2}} \left(\frac{1+z}{1+10}\right)^3 \, {\rm s}^{-1}. \tag{A.65}$$

We can also similarly work out the temperature evolution of the hydrogen kinetic temperature,

$$\frac{dT_K}{dt} = -2HT_\chi + \Gamma_c(T_{\rm CMB} - T_K) + \frac{2}{3}\dot{Q}_H, \tag{A.66}$$

where the second term is the heating due to CMB and Γ_c is the compton rate, which depends on the free electron fraction. In the last term $\dot{Q}_H$ is the energy transfer rate from the dark matter fluid to the gas, which can be related to the heating rate of the DM $\dot{Q}_\chi$ as,

$$\dot{Q}_H = -\frac{n_\chi}{n_H}\dot{Q}_\chi, \tag{A.67}$$

$$= \Gamma_H(T_\chi - T_K), \tag{A.68}$$

where we have defined the rate constant Γ_H as,

$$\Gamma_H = n_\chi \left(\frac{\Delta\mu}{2MT_{\rm eff}}\right) \frac{3}{4\pi} \frac{g_\chi^2 g_e^2}{\Delta^2} \sqrt{\frac{8T_{\rm eff}}{\pi\mu}},$$

$$= 2.05 \times 10^{-39} \left(\frac{f}{0.1}\right) \left(\frac{0.1\,{\rm GeV}}{m_\chi}\right) \left(\frac{\alpha_\chi}{10^{-2}}\right) \left(\frac{\alpha_e}{10^{-14}}\right) \left(\frac{1\,{\rm GeV}}{M}\right) \left(\frac{\mu}{0.1\,{\rm GeV}}\right)^{\frac{1}{2}} \left(\frac{10\,{\rm K}}{T_{\rm eff}}\right)^{\frac{1}{2}} \left(\frac{1+z}{1+10}\right)^3 \, {\rm GeV},$$

$$= 3.11 \times 10^{-15} \left(\frac{f}{0.1}\right) \left(\frac{0.1\,{\rm GeV}}{m_\chi}\right) \left(\frac{\alpha_\chi}{10^{-2}}\right) \left(\frac{\alpha_e}{10^{-14}}\right) \left(\frac{1\,{\rm GeV}}{M}\right) \left(\frac{\mu}{0.1\,{\rm GeV}}\right)^{\frac{1}{2}} \left(\frac{10\,{\rm K}}{T_{\rm eff}}\right)^{\frac{1}{2}} \left(\frac{1+z}{1+10}\right)^3 \, {\rm s}^{-1}, \tag{A.69}$$

B Elastic scattering energy-transfer cross-section

We discuss here the forward scattering divergence of elastic scattering for processes such as $\chi + H_1 \to \chi + H_1$, $\chi + e^- \to \chi + e^-$ and $\chi + \chi \to \chi + \chi$. The energy transfer cross-section for each of these processes can be defined as follows,

$$\bar{\sigma} = \int d\Omega \frac{d\sigma}{d\Omega}(1 - \cos\theta), \tag{B.1}$$

the integral over the polar scattering angle takes the form,

$$\mathcal{I} = \int_{-1}^{1} d\cos\theta \frac{(1 - \cos\theta)}{\left(1 - \cos\theta + \frac{m_V^2}{2p^2}\right)^2} \tag{B.2}$$

$$= \text{Log}\left(1 + \frac{4p^2}{m_V^2}\right) - \frac{1}{1 + \frac{m_V^2}{4p^2}} \tag{B.3}$$

$$\xrightarrow[m_V \to 0]{} \text{Log}\left(\frac{4p^2}{m_V^2}\right), \tag{B.4}$$

where $p = \mu v$ is the relative momentum of the incoming particles, μ being the reduced mass and v the relative velocity of the incoming particles. In the last expression we have taken the limit of small mediator mass, $m_V \to 0$. For elastic scattering, the forward divergence in the energy transfer cross-section is cut-off by the mediator mass and this gives rise to a logarithmic divergence. Similar expressions can be found in the literature, for example see ref. [61] for DM elastic scattering through a light mediator.

For completeness, we present here the various energy transfer cross-sections for elastic scattering processes.

The process $\chi + e^- \to \chi + e^-$ is important for determining the pre-recombination initial conditions on the DM temperature. The energy transfer cross-section for this process is given by,

$$\bar{\sigma}(\chi + e^- \to \chi + e^-) = \frac{3}{8\pi} \frac{g_\chi^2 g_e^2}{\mu_{\chi e}^2 v^4} \text{Log}\left(\frac{4\mu_{\chi e}^2 v^2}{m_V^2}\right), \tag{B.5}$$

where $\mu_{\chi e}$ is the reduced mass of the DM and electron.

DM self-scattering $\chi + \chi \to \chi + \chi$ is important when considering astrophysical self-interaction constraints. For this process the energy transfer cross-section is given by,

$$\bar{\sigma}(\chi + \chi \to \chi + \chi) \sim \frac{3}{2\pi} \frac{g_\chi^4}{m_\chi^2 v^4} \text{Log}\left(\frac{m_\chi^2 v^2}{m_V^2}\right). \tag{B.6}$$

Finally, for elastic $\chi + H_1 \to \chi + H_1$ scattering, which only proceeds through the $s'_H = \pm 1$ states of H_1 without flipping the spin, we have the energy transfer cross-section of the form,

$$\bar{\sigma}(\chi + H_1 \to \chi + H_1) = \frac{1}{24\pi} \frac{g_\chi^2 g_e^2}{\mu^2 v^4} \text{Log}\left(\frac{4\mu^2 v^2}{m_V^2}\right), \tag{B.7}$$

where μ is the reduced mass of the DM and hydrogen.

References

[1] J.R. Pritchard and A. Loeb, *21 cm cosmology in the 21st century*, *Reports on Progress in Physics* **75** (2012) 086901 [1109.6012].

[2] G.B. Field, *Excitation of the Hydrogen 21-CM Line*, *Proceedings of the IRE* **46** (1958) 240.

[3] S. Furlanetto, *The Global 21 Centimeter Background from High Redshifts*, *Mon. Not. Roy. Astron. Soc.* **371** (2006) 867 [astro-ph/0604040].

[4] R. Barkana and A. Loeb, *Detecting the earliest galaxies through two new sources of 21cm fluctuations*, *Astrophys. J.* **626** (2005) 1 [astro-ph/0410129].

[5] S.A. Wouthuysen, *On the excitation mechanism of the 21-cm (radio-frequency) interstellar hydrogen emission line.*, *Astronomical Journal* **57** (1952) 31.

[6] J.R. Pritchard and A. Loeb, *21-cm cosmology*, *Rept. Prog. Phys.* **75** (2012) 086901 [1109.6012].

[7] R. Barkana, *The Rise of the First Stars: Supersonic Streaming, Radiative Feedback, and 21-cm Cosmology*, *Phys. Rept.* **645** (2016) 1 [1605.04357].

[8] S.R. Furlanetto, *The Fundamentals of the 21-cm Line*, 1909.13740.

[9] J.D. Bowman and A.E.E. Rogers, *A lower limit of dz > 0.06 for the duration of the reionization epoch*, *Nature* **468** (2010) 796 [1209.1117].

[10] L. Philip, Z. Abdurashidova, H.C. Chiang, N. Ghazi, A. Gumba, H.M. Heilgendorff et al., *Probing radio intensity at high-z from marion: 2017 instrument*, *Journal of Astronomical Instrumentation* **08** (2019) 1950004.

[11] "Reach project homepage." https://www.astro.phy.cam.ac.uk/news/REACH.

[12] N. Patra, R. Subrahmanyan, A. Raghunathan and N. Udaya Shankar, *Saras: a precision system for measurement of the cosmic radio background and signatures from the epoch of reionization*, *Experimental Astronomy* **36** (2013) 319–370.

[13] S. Singh, R. Subrahmanyan, N.U. Shankar, M.S. Rao, B.S. Girish, A. Raghunathan et al., *SARAS 2: A Spectral Radiometer for probing Cosmic Dawn and the Epoch of Reionization through detection of the global 21 cm signal*, *Exper. Astron.* **45** (2018) 269 [1710.01101].

[14] T.C. Voytek, A. Natarajan, J.M.J. García, J.B. Peterson and O. López-Cruz, *PROBING THE DARK AGES AT z ∼ 20: THE SCI-HI 21 cm ALL-SKY SPECTRUM EXPERIMENT*, *The Astrophysical Journal* **782** (2014) L9.

[15] M. Sokolowski, S.E. Tremblay, R.B. Wayth, S.J. Tingay, N. Clarke, P. Roberts et al., *Bighorns - broadband instrument for global hydrogen reionisation signal*, *Publications of the Astronomical Society of Australia* **32** (2015) .

[16] L.J. Greenhill and G. Bernardi, *HI epoch of reionization arrays*, 1201.1700.

[17] X. Chen, J. Burns, L. Koopmans, H. Rothkaehi, J. Silk, J. Wu et al., *Discovering the Sky at the Longest Wavelengths with Small Satellite Constellations*, *arXiv e-prints* (2019) arXiv:1907.10853 [1907.10853].

[18] J. Burns, G. Hallinan, J. Lux, A. Romero-Wolf, T.-C. Chang, J. Kocz et al., *Farside: A low radio frequency interferometric array on the lunar farside*, 2019.

[19] "Pratush project homepage." http://www.rri.res.in/DISTORTION/pratush.html.

[20] D.L. Jones, T.J.W. Lazio and J.O. Burns, *Dark ages radio explorer mission: Probing the cosmic dawn*, *2015 IEEE Aerospace Conference* (2015) .

[21] L. Chen, J. Ping, H. Falcke, M.K. Wolt and N. Team, *The netherlands-china low frequency explorer (ncle)*, *Bulletin of the AAS* **52** (2020) .

[22] L. Koopmans, R. Barkana, M. Bentum, G. Bernardi, A.-J. Boonstra, J. Bowman et al., *Peering into the Dark (Ages) with Low-Frequency Space Interferometers*, *arXiv e-prints* (2019) arXiv:1908.04296 [`1908.04296`].

[23] J.O. Burns et al., *Dark Cosmology: Investigating Dark Matter \& Exotic Physics in the Dark Ages using the Redshifted 21-cm Global Spectrum*, `1902.06147`.

[24] H.J.A. Rottgering, R. Braun, P.D. Barthel, M.P. van Haarlem, G.K. Miley, R. Morganti et al., *LOFAR - Opening up a new window on the Universe*, in *Conference on Cosmology, Galaxy Formation and Astro-Particle Physics on the Pathway to the SKA*, 10, 2006 [`astro-ph/0610596`].

[25] A.R. Parsons, D.C. Backer, G.S. Foster, M.C.H. Wright, R.F. Bradley, N.E. Gugliucci et al., *The precision array for probing the epoch of re-ionization: Eight station results*, *The Astronomical Journal* **139** (2010) 1468–1480.

[26] S.J. Tingay, R. Goeke, J.D. Bowman, D. Emrich, S.M. Ord, D.A. Mitchell et al., *The murchison widefield array: The square kilometre array precursor at low radio frequencies*, *Publications of the Astronomical Society of Australia* **30** (2013) .

[27] Q. Zheng, X.-P. Wu, M. Johnston-Hollitt, J. hua Gu and H. Xu, *RADIO SOURCES IN THE NCP REGION OBSERVED WITH THE 21 CENTIMETER ARRAY*, *The Astrophysical Journal* **832** (2016) 190.

[28] M. Eastwood, M. Anderson, R. Monroe, G. Hallinan, M. Catha, J. Dowell et al., *The 21 cm power spectrum from the cosmic dawn: First results from the OVRO-LWA*, *arXiv: Cosmology and Nongalactic Astrophysics* (2019) .

[29] U.-L. Pen, T.-C. Chang, C.M. Hirata, J.B. Peterson, J. Roy, Y. Gupta et al., *The GMRT EoR experiment: limits on polarized sky brightness at 150 MHz*, *Monthly Notices of the Royal Astronomical Society* **399** (2009) 181.

[30] D.R.D. et al., *Hydrogen epoch of reionization array (HERA)*, *Publications of the Astronomical Society of the Pacific* **129** (2017) 045001.

[31] M.G. et al., *Reionization and the cosmic dawn with the square kilometre array*, *Experimental Astronomy* **36** (2013) .

[32] L.V.E. Koopmans et al., *The Cosmic Dawn and Epoch of Reionization with the Square Kilometre Array*, *PoS* **AASKA14** (2015) 001 [`1505.07568`].

[33] J.D. Bowman, A.E.E. Rogers, R.A. Monsalve, T.J. Mozdzen and N. Mahesh, *An absorption profile centred at 78 megahertz in the sky-averaged spectrum*, *Nature* **555** (2018) 67 [`1810.05912`].

[34] R. Barkana, *Possible interaction between baryons and dark-matter particles revealed by the first stars*, *Nature* **555** (2018) 71 [`1803.06698`].

[35] J.B. Muñoz and A. Loeb, *A small amount of mini-charged dark matter could cool the baryons in the early Universe*, *Nature* **557** (2018) 684 [`1802.10094`].

[36] A. Berlin, D. Hooper, G. Krnjaic and S.D. McDermott, *Severely Constraining Dark Matter Interpretations of the 21-cm Anomaly*, *Phys. Rev. Lett.* **121** (2018) 011102 [`1803.02804`].

[37] R. Barkana, N.J. Outmezguine, D. Redigolo and T. Volansky, *Strong constraints on light dark matter interpretation of the EDGES signal*, *Phys. Rev.* **D98** (2018) 103005 [`1803.03091`].

[38] E.D. Kovetz, V. Poulin, V. Gluscevic, K.K. Boddy, R. Barkana and M. Kamionkowski, *Tighter limits on dark matter explanations of the anomalous EDGES 21 cm signal*, *Phys. Rev.* **D98** (2018) 103529 [`1807.11482`].

[39] L.-B. Jia, X.-J. Deng and C.-F. Liu, *Could the 21-cm absorption be explained by the dark matter suggested by*[8] *Be transitions?*, *Eur. Phys. J.* **C78** (2018) 956 [`1809.00177`].

[40] N. Klop and S. Ando, *Constraints on MeV dark matter using neutrino detectors and their implication for the 21-cm results*, *Phys. Rev.* **D98** (2018) 103004 [1809.00671].

[41] H. Liu, N.J. Outmezguine, D. Redigolo and T. Volansky, *Reviving Millicharged Dark Matter for 21-cm Cosmology*, *Phys. Rev. D* **100** (2019) 123011 [1908.06986].

[42] C. Creque-Sarbinowski, L. Ji, E.D. Kovetz and M. Kamionkowski, *Direct millicharged dark matter cannot explain the edges signal*, *Phys. Rev. D* **100** (2019) 023528.

[43] N. Houston, C. Li, T. Li, Q. Yang and X. Zhang, *Natural Explanation for 21 cm Absorption Signals via Axion-Induced Cooling*, *Phys. Rev. Lett.* **121** (2018) 111301 [1805.04426].

[44] P. Sikivie, *Axion dark matter and the 21-cm signal*, *Phys. Dark Univ.* **24** (2019) 100289 [1805.05577].

[45] M. Pospelov, J. Pradler, J.T. Ruderman and A. Urbano, *Room for New Physics in the Rayleigh-Jeans Tail of the Cosmic Microwave Background*, *Phys. Rev. Lett.* **121** (2018) 031103 [1803.07048].

[46] T. Moroi, K. Nakayama and Y. Tang, *Axion-photon conversion and effects on 21 cm observation*, *Phys. Lett. B* **783** (2018) 301 [1804.10378].

[47] S. Fraser et al., *The EDGES 21 cm Anomaly and Properties of Dark Matter*, *Phys. Lett. B* **785** (2018) 159 [1803.03245].

[48] K. Bondarenko, J. Pradler and A. Sokolenko, *Constraining dark photons and their connection to 21 cm cosmology with CMB data*, *Phys. Lett. B* **805** (2020) 135420 [2002.08942].

[49] N. Brahma, S. Sethi and S. Sista, *Energy injection in pre-recombination era and EDGES detection*, 2007.06417.

[50] A. Falkowski and K. Petraki, *21cm absorption signal from charge sequestration*, 1803.10096.

[51] R. Hills, G. Kulkarni, P.D. Meerburg and E. Puchwein, *Concerns about modelling of the EDGES data*, *Nature* **564** (2018) E32 [1805.01421].

[52] A. Caputo, H. Liu, S. Mishra-Sharma, M. Pospelov, J.T. Ruderman and A. Urbano, *Edges and Endpoints in 21-cm Observations from Resonant Photon Production*, 2009.03899.

[53] G. Lambiase and S. Mohanty, *Hydrogen spin oscillations in a background of axions and the 21-cm brightness temperature*, *Mon. Not. Roy. Astron. Soc.* **494** (2020) 5961 [1804.05318].

[54] A. Auriol, S. Davidson and G. Raffelt, *Axion absorption and the spin temperature of primordial hydrogen*, *Phys. Rev.* **D99** (2019) 023013 [1808.09456].

[55] A. Widmark, *21 cm cosmology and spin temperature reduction via spin-dependent dark matter interactions*, *JCAP* **1906** (2019) 014 [1902.09552].

[56] Y. Ali-Haïmoud and C.M. Hirata, *Ultrafast effective multilevel atom method for primordial hydrogen recombination*, *Phys. Rev. D* **82** (2010) 063521 [1006.1355].

[57] C.-P. Ma and E. Bertschinger, *Cosmological perturbation theory in the synchronous and conformal Newtonian gauges*, *Astrophys. J.* **455** (1995) 7 [astro-ph/9506072].

[58] PLANCK collaboration, *Planck 2018 results. VI. Cosmological parameters*, *Astron. Astrophys.* **641** (2020) A6 [1807.06209].

[59] S. Mittal and G. Kulkarni, *Lyman-α coupling and heating at Cosmic Dawn*, 2009.10746.

[60] J. Mirocha and S.R. Furlanetto, *What does the first highly-redshifted 21-cm detection tell us about early galaxies?*, *Mon. Not. Roy. Astron. Soc.* **483** (2019) 1980 [1803.03272].

[61] S. Tulin, H.-B. Yu and K.M. Zurek, *Beyond Collisionless Dark Matter: Particle Physics Dynamics for Dark Matter Halo Structure*, *Phys. Rev. D* **87** (2013) 115007 [1302.3898].

[62] D. Tseliakhovich and C. Hirata, *Relative velocity of dark matter and baryonic fluids and the formation of the first structures*, *Phys. Rev. D* **82** (2010) 083520 [`1005.2416`].

[63] Y. Ali-Haïmoud, P.D. Meerburg and S. Yuan, *New light on 21 cm intensity fluctuations from the dark ages*, *Phys. Rev. D* **89** (2014) 083506 [`1312.4948`].

[64] J.B. Muñoz, E.D. Kovetz and Y. Ali-Haïmoud, *Heating of Baryons due to Scattering with Dark Matter During the Dark Ages*, *Phys. Rev. D* **92** (2015) 083528 [`1509.00029`].

[65] S. Karshenboim, *Constraints on a long-range spin-dependent interaction from precision atomic physics*, *Phys. Rev. D* **82** (2010) 113013 [`1005.4868`].

[66] M. Jiao, X. Rong, H. Liang, Y.-F. Cai and J. Du, *Searching for an Exotic Spin-Dependent Interaction between Electrons at the Nanometer Scale with Molecular Rulers*, *Phys. Rev. D* **101** (2020) 115011 [`1904.09428`].

[67] S. Kotler, R. Ozeri and D.F.J. Kimball, *Constraints on exotic dipole-dipole couplings between electrons at the micrometer scale*, *Phys. Rev. Lett.* **115** (2015) 081801 [`1501.07891`].

[68] X. Rong, M. Jiao, J. Geng, B. Zhang, T. Xie, F. Shi et al., *Constraints on a Spin-Dependent Exotic Interaction between Electrons with Single Electron Spin Quantum Sensors*, *Phys. Rev. Lett.* **121** (2018) 080402 [`1804.07026`].

[69] J. Preskill, *Gauge anomalies in an effective field theory*, *Annals Phys.* **210** (1991) 323.

[70] J.A. Dror, R. Lasenby and M. Pospelov, *New constraints on light vectors coupled to anomalous currents*, *Phys. Rev. Lett.* **119** (2017) 141803 [`1705.06726`].

[71] J.A. Dror, R. Lasenby and M. Pospelov, *Dark forces coupled to nonconserved currents*, *Phys. Rev. D* **96** (2017) 075036 [`1707.01503`].

[72] L3 collaboration, *Search for new physics in energetic single photon production in e^+e^- annihilation at the Z resonance*, *Phys. Lett. B* **412** (1997) 201.

[73] DELPHI collaboration, *Photon events with missing energy in e+ e- collisions at s**(1/2) = 130-GeV to 209-GeV*, *Eur. Phys. J. C* **38** (2005) 395 [`hep-ex/0406019`].

[74] M. Giannotti, I.G. Irastorza, J. Redondo, A. Ringwald and K. Saikawa, *Stellar Recipes for Axion Hunters*, *JCAP* **10** (2017) 010 [`1708.02111`].

[75] I.G. Irastorza and J. Redondo, *New experimental approaches in the search for axion-like particles*, *Prog. Part. Nucl. Phys.* **102** (2018) 89 [`1801.08127`].

[76] P. Jain and S. Mandal, *Evading the astrophysical limits on light pseudoscalars*, *Int. J. Mod. Phys. D* **15** (2006) 2095 [`astro-ph/0512155`].

[77] E. Masso and J. Redondo, *Evading astrophysical constraints on axion-like particles*, *JCAP* **09** (2005) 015 [`hep-ph/0504202`].

[78] W. DeRocco, P.W. Graham and S. Rajendran, *Exploring the robustness of stellar cooling constraints on light particles*, *Phys. Rev. D* **102** (2020) 075015 [`2006.15112`].

[79] R. Budnik, H. Kim, O. Matsedonskyi, G. Perez and Y. Soreq, *Probing the relaxed relaxion and Higgs-portal with S1 \& S2*, `2006.14568`.

[80] I.M. Bloch, A. Caputo, R. Essig, D. Redigolo, M. Sholapurkar and T. Volansky, *Exploring New Physics with O(keV) Electron Recoils in Direct Detection Experiments*, `2006.14521`.

[81] B.D. Fields, K.A. Olive, T.-H. Yeh and C. Young, *Big-Bang Nucleosynthesis After Planck*, *JCAP* **03** (2020) 010 [`1912.01132`].

[82] C.D. Kreisch, F.-Y. Cyr-Racine and O. Doré, *Neutrino puzzle: Anomalies, interactions, and cosmological tensions*, *Phys. Rev. D* **101** (2020) 123505 [`1902.00534`].

[83] S. Dubovsky, D. Gorbunov and G. Rubtsov, *Narrowing the window for millicharged particles by CMB anisotropy*, *JETP Lett.* **79** (2004) 1 [`hep-ph/0311189`].

[84] K.K. Boddy and V. Gluscevic, *First Cosmological Constraint on the Effective Theory of Dark Matter-Proton Interactions*, *Phys. Rev. D* **98** (2018) 083510 [`1801.08609`].

[85] K.K. Boddy, V. Gluscevic, V. Poulin, E.D. Kovetz, M. Kamionkowski and R. Barkana, *Critical assessment of CMB limits on dark matter-baryon scattering: New treatment of the relative bulk velocity*, *Phys. Rev. D* **98** (2018) 123506 [`1808.00001`].

[86] S. Tulin and H.-B. Yu, *Dark Matter Self-interactions and Small Scale Structure*, *Phys. Rept.* **730** (2018) 1 [`1705.02358`].

[87] G. Kulkarni, J.F. Hennawi, J. Oñorbe, A. Rorai and V. Springel, *Characterizing the Pressure Smoothing Scale of the Intergalactic Medium*, *Astrophysical Journal* **812** (2015) 30 [`1504.00366`].

[88] A. Rorai, J.F. Hennawi, J. Oñorbe, M. White, J.X. Prochaska, G. Kulkarni et al., *Measurement of the small-scale structure of the intergalactic medium using close quasar pairs*, *Science* **356** (2017) 418 [`1704.08366`].

[89] M. Cirelli, E. Del Nobile and P. Panci, *Tools for model-independent bounds in direct dark matter searches*, *JCAP* **1310** (2013) 019 [`1307.5955`].